DEEP UV RAMAN SPECTROSCOPY

by

RAJ PATIL

A Thesis Submitted to the Faculty of the

COLLEGE OF OPTICAL SCIENCES

In Partial Fulfillment of the Requirements

For the Degree of

MASTER OF SCIENCE

In the Graduate College

THE UNIVERSITY OF ARIZONA

2016

STATEMENT BY AUTHOR

The thesis titled *DEEP UV RAMAN SPECTROSCOPY* prepared by *RAJ PATIL* has been submitted in partial fulfillment of requirements for a master's degree at the University of Arizona and is deposited in the University Library to be made available to borrowers under rules of the Library.

Brief quotations from this thesis are allowable without special permission, provided that an accurate acknowledgement of the source is made. Requests for permission for extended quotation from or reproduction of this manuscript in whole or in part may be granted by the head of the major department or the Dean of the Graduate College when in his or her judgment the proposed use of the material is in the interests of scholarship. In all other instances, however, permission must be obtained from the author.

SIGNED: *RAJ PATIL*

APPROVAL BY THESIS DIRECTOR

This thesis has been approved on the date shown below:

KHANH KIEU
Professor of College of Optical Sciences

04-27-16
Date

Acknowledgements

I would like to thank my advisor Prof. Khanh Kieu for his guidance throughout my research for the thesis. I would like to thank Dr. Palash Gangopadhyay for providing me with carbon nanotubes (CNTs) samples for Raman spectroscopy. I would like to thank all of the group members Joshua, Soroush, Babak, Dawson, Roopa, Neil and Dmitriy. A special thanks to my friends Soha, Phillip, and Alexander for the insightful discussions. Lastly I want to thank my parents for their continuous support and encouragement in pursuing my career.

Dedication

Dedicated to my Parents.....

Contents

List of Figures

Physical Constants

Speed of Light	$c = 2.997\,924\,58 \times 10^{8}\,\mathrm{m\,s^{-1}}$
Boltzmann Constant	$K = 1.380\,648\,52 \times 10^{-23}\,\mathrm{kgm^{2}s^{-2}K^{-1}}$
Planck Constant	$h = 6.626\,070\,04 \times 10^{-34}\,\mathrm{kgm^{2}s^{-1}}$
Electron Charge	$e = -1.602\,176\,62 \times 10^{-19}\,\mathrm{A\,s}$

THE UNIVERSITY OF ARIZONA

Abstract

Dr. Khanh Kieu
College of Optical Sciences

Masters of Science

DEEP UV RAMAN SPECTROSCOPY

by Raj PATIL

This thesis examines the performance of a custom built deep UV laser (257.5 nm) for Raman spectroscopy and the advantages of Raman spectroscopy with a laser in the deep UV over a laser in the visible range (532 nm). It describes the theory of resonance Raman scattering, the experimental setup for Raman spectroscopy and a few Raman spectroscopy measurements. The measurements were performed on biological samples oak tree leaf and lactobacillus acidophilus and bifidobacteria from probotioc medicinal capsules. Fluorescence free Raman spectra were acquired for the two samples with 257.5 nm laser. The Raman spectra for the two samples with a 532 nm laser was masked with fluorescence. Raman measurements for an inorganic salt sodium nitrate showed a resonance Raman effect with 257.5 nm laser which led to enhancement in the Raman intensity as compared to that with 532 nm laser. Therefore we were able to demonstrate two advantages of deep UV Raman spectroscopy. First one is the possibility of acquiring fluorescence free spectra for biological samples. Second is the possibility of gaining enhancement in Raman intensity due to resonance Raman effect. It was observed that 257.5 nm laser requires optimization to reduce the bandwidth of the laser to get better resolution. The 257.5 nm laser also needs to be optimized to obtain higher power to get better signal to noise ratio. The experimental setup can also be further improved to obtain better resolution. If the improvements required in the setup are implemented, the deep UV Raman setup will become an important tool for spectroscopy. ...

Chapter 1

Introduction

Raman spectroscopy has become an important tool in investigating the molecular structure of a material. Indeed, the Raman spectrum is a direct signature of the material. It does not require any external markers. It provides an opportunity to do marker free imaging and sensing in various fields. It has been used in biomedical Imaging, purity testing of materials(adulteration), photolithography , wafer inspection, studying molecular structure of materials, etc. Lasers in the near infrared, visible and ultraviolet range have been used in Raman spectroscopy. But lasers in deep UV provide some specific advantages over lasers in the visible range. They provide fluorescence free Raman spectra and enhancement in the intensity of the Raman signal.

Raman scattering or the Raman effect was discovered by C. V. Raman and K. S. Krishnan in liquids [1] and by G. Landsberg and L. I. Mandelstam in crystals. The effect had been predicted theoretically by Adolf Smekal in 1923 [2]. In 1953 the first resonance Raman spectra was reported by Shorygin, and since then the use of resonance enhancement to improve the sensitivity of Raman spectroscopy has become a very popular technique, in particular for those researchers interested in biological problems. The Resonance Raman measurements have been carried out on different materials with the introduction of the lasers at new wavelengths over time. The report by Asher, S.A. [3] acted as a starting point for research for this thesis. The report briefly introduces the theory about UV resonance Raman spectroscopy (UVRSS), its instrumentation and its application in analytical, physical, and biophysical Chemistry. Resonance Raman spectroscopy depends on the wavelength of the laser being used to probe the material. If the

wavelength is in resonance with one of the absorption bands in the material , we see enhancement in the Raman signal which is known as resonance Raman scattering. Most of the bio-molecules have their absorption bands in the deep UV. Hence we can obtain the resonance Raman effect in Deep UV for bio-molecules. It was further established by Asher et.al.[4] that fluorescence interference is minimized with ultraviolet excitation below 260 nm(Deep UV). 257.26 nm excitation from an intracavity doubled argon-ion laser was used to distinguish normal from malignant cultured breast and cervical cells [5]. UV resonance Raman spectroscopy of DNA and protein constituents of viruses was performed with excitations at 257, 244, 238, and 229 nm [6]. Deep UV lasers have been used for performing fluorescence free Raman spectroscopy of many more bio-molecules.

Presently gas lasers, laser diodes and solid-state lasers are being employed to generate wavelengths from 120 nm XUV to UV 400 nm. We have developed a compact deep UV (< 300 nm) light source based on the paper [7] published by our group using fiber laser technology via second harmonic frequency conversion processes. The advantages of this source are all-fiber design, compact, maintenance free, short wavelength 257.5 nm (DUV), short pulse (6 ps), high repetition rate (60MHz) and not too expensive. We have employed this laser for performing Raman measurements. We were able to demonstrate fluorescence free Raman measurements for bio molecules. We were also able to demonstrate resonant enhancement for an inorganic salt sodium nitrate.

In this thesis we will discuss the physics of Raman spectroscopy, the experimental setup for Raman measurements in great detail and describe few Raman measurement results. We will establish and demonstrate the advantages of deep UV laser for Raman spectroscopy.

In Chapter 2, we discuss the theory behind Raman spectroscopy. We will discuss the general polarizability theory of Raman scattering and Placzeks simplified polarizability theory. Then we will consider how the equations from the above theories modify for resonant Raman scattering. We will also

discuss how the fluorescence process masks the Raman spectra and establish the fact that the Raman laser in deep UV provides a fluorescence free Raman spectra and we can obtain resonant enhancement in the intensity of the Raman signal as compared to that of visible laser.

In Chapter 3, we have gone through in great detail about the design of the optical setup for Raman measurements. The process of designing and selection for each component of the setup had been discussed and evaluated. The specifications and the relevant graphs of the commercial components used in the setup have been stated and explained in the thesis. The features of the custom made LABVIEW program have been listed at the end of the Chapter 3.

In Chapter 4, we discuss about the Raman measurements for silicon, distilled water, bio-molecules (oak tree leaf and lactobacillus acidophilus and bifidobacteria from a probotioc medicinal Capsules) and the inorganic salt sodium nitrate $NaNO_3$. We also performed polarized Raman measurements for SWCNTS (Single walled Carbon Nanotubes).

In the end we have evaluated the advantages and shortcomings of the custom built Deep UV laser for Raman spectroscopy. We also provide possible solutions to overcome these shortcomings and drawn out future plans to resolve these shortcomings.

Chapter 2

Theory

2.1 Raman Scattering

The Molecules scatter light when light is incident on them. If the frequency of the scattered light is same as that of the input light we call it Rayleigh scattering. If the frequency of the scattered light is not the same, it is known as Raman scattering. The change in the frequency is due to the coupling of the incident light with the vibrational-rotational states of the molecules. To calculate the intensities of Raman scattering and to understand what these intensities depend on, its imperative to understand the quantum mechanical theory of Rayleigh scattering. This will act as the starting point for understanding Raman scattering and we will develop more concise and simple theory in later stages, which we can apply for simple cases of Raman scattering in molecules and atoms.

The atomic or molecular energy structure is made up of many energy levels. These energy levels consist of purely electronic levels, superimposed by vibrational levels. These vibrational levels are further superimposed by rotational energy levels. These vibrational and rotational levels corresponding to an electronic state are collectively referred to as energy manifold. The vibrational and rotational levels can be Raman scattering is due to coupling of an external electric field (v_o) with the vibrational and rotational energy levels of the **bonds** formed between atoms and molecules.

The energy levels in a bond can be described using the Morse potential

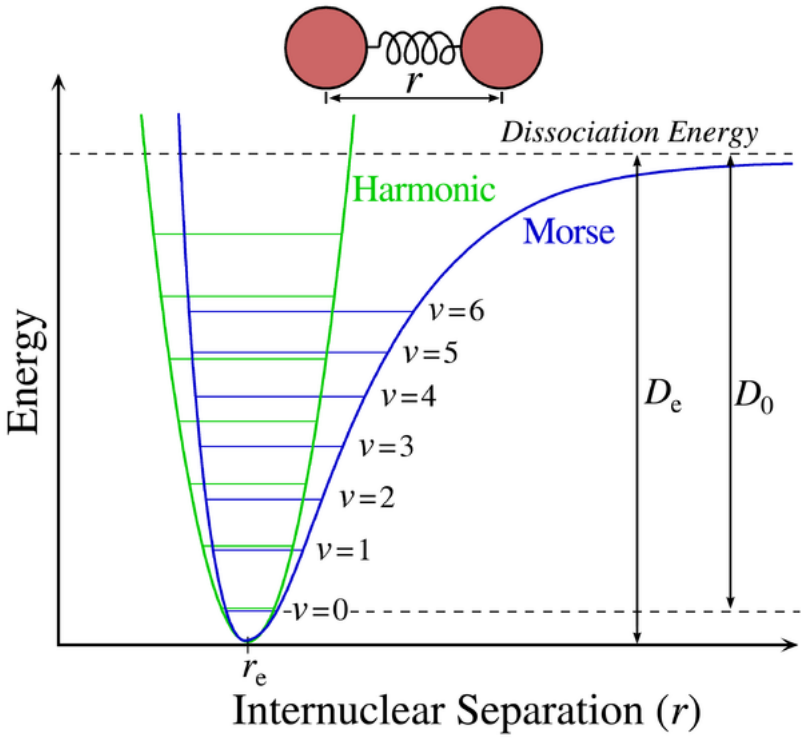

H

FIGURE 2.1: Morse potential energy curve *(Morse-potential.png, Attribution :Samoza, wikimedia.org)*

energy curve shown in Figure 2.1. The bond between two atoms can be described as two entities of masses m_1 and m_2 connected by a spring. At equilibrium the distance between them is r_e. The energy corresponding to this separation is the bond energy. But due to the wave nature of the electrons, the bond has some vibrational energy, defined as the zeroth vibrational energy. The quantum harmonic oscillator model lacks an explanation for the formation and dissociation of the bond. Hence, the Morse energy curve is preferred. As expected, with the decrease in the inter-nuclear separation the energy goes to infinity due to the nuclear forces. As the inter-nuclear separation distance increases, the potential energy goes on increasing. But the potential energy curve approaches asymptotically to the dissociation energy D_e (bond breaks). Just like the quantum harmonic oscillator model, it also allows definite energy levels which are known as vibrational levels. The difference between the energy levels goes on decreasing with increasing energy.

The Morse energy curve can be described by (2.1)

$$V(r) = D_e(1 - e^{-a(r-r_e)})^2 \tag{2.1}$$

where a controls the width of the curve and is given by (2.2)

$$a = \sqrt{\frac{k_e}{2D_e}} \tag{2.2}$$

where k_e is the force constant at the minimum of the well. The force constant of the bond can be found by Taylor expansion of $V(r)$ around $r = r_e$ to the second derivative of the potential energy function. The spacing between the energy levels is given by (2.3)

$$E(i+1) - E(i) = hv_f - (i+1)(hv_f)^2/2D_e \tag{2.3}$$

where v_f is called the fundamental frequency of the vibration and given by (2.4)

$$v_f = \frac{a}{2}\sqrt{2D_e/m} \tag{2.4}$$

where m is the reduced mass $m = \frac{m_1 m_2}{m_1+m_2}$. v_f depends uniquely on the parameters of the bond . When an electron is excited to a higher energy level from the zeroth vibrational state $f = 0$, the excited electron can relax back to $f = 0, 1, 2, 3, ...$ For $f \neq 0$, we get Raman scattering. This shift in the energy level in this transition, can be related to a wavenumber shift by $\frac{1}{\lambda_o} - \frac{1}{\lambda_f}$. This is called the Raman shift and has units of cm^{-1}. For $f = 1$, the shift is called the fundamental shift, while for $f = 2, 3, 4$ we get overtones. So qualitatively, we have discussed the way we obtain Raman scattering spectra and its dependence on the parameters of the bond. Next, we will discuss about how to determine the intensity of the Raman spectra.

2.1.1 Quantum Mechanical Theory of Light Scattering

(2.5) gives the intensity I_{nm} of the Raman scattering for particular frequency v_{nm} corresponding to transition between m and n. m and n are the initial and final vibrational states, v_o is the incident frequency, P_{nm} is the induced electric moment matrix and C is a constant.

$$I_{nm} = C(v_o + v_{nm})P_{nm}^2 \tag{2.5}$$

Constant C is equal to $64\pi^2/(3c^2)$, where c is the speed of the light. v_{nm} is the vibration frequency given by equation (2.6), E_i corresponding the energy level of that state and h is the Plancks constant.

$$v_{nm} = (E_n - E_m)/h \tag{2.6}$$

If we define ψ_n and ψ_m to be the time independent wavefunctions of the states n and m respectively, then P_{nm} is given by (2.7), where P is the induced dipole moment.

$$P_{nm} = \int \psi_n^* P \psi_m d\tau \tag{2.7}$$

Lets consider a free molecule with no external fields and let r be the total no. of states. Lets consider an electron which undergoes a transition from initial state m to the final state n (one of the r states).The quantum mechanical result for P_{nm} is given by (2.8)

$$P_{nm} = \sum_i^r \left(\frac{M_{mi}M_{in}}{v_{im} - v_o} + \frac{M_{ni}M_{im}}{v_{in} + v_o}\right)\frac{E}{h} \tag{2.8}$$

where M_{ji} is the induced dipole moment. There is a tricky part which needs to be understood. For Raman scattering to take place, the excited state can be real or virtual. Here a real state means an actual state present in the atom and a virtual state means an imaginary state which is taken in to consideration to explain the Raman scattering process. Hence, for Raman scattering process to take place, a real excited state is not necessarily

required, as the process is considered to be instantaneous. The lifetime of the process is in the order of few pico-seconds.

Another subtle point which needs to be understood is that the electron does not necessarily transit over all the r states as suggested by (2.8). The summation over these r states just comes out of the need of the representation of the wavefunction with a complete set of states. These equations clearly look complex and difficult to manipulate but we can simplify them and employ much simpler formulas, which will be elucidated in the next sections.

2.1.2 Stokes and Anti-Stokes Scattering

Raman scattering can be divided into Stokes and anti-Stokes scattering. For anti-Stokes scattering, the scattered frequency is higher than the incident frequency. Here the initial state lies above the final state. For Stokes scattering, the scattered frequency is lower than the incident frequency. The initial state lies below the final state. The intensity of Stokes scattering is generally more than anti-Stokes scattering.

The intial state (m2) for the anti-Stokes scattering is at a higher energy level as compared to the vibrational state (m1) of the Stokes scattering. The population ratio for these two initial states is given by the Boltzmann distribution (2.9).

$$\frac{P(anti-stokes_{m2})}{P(stokes_{m1})} = e^{-\frac{E_{m2}-E_{m1}}{KT}} \tag{2.9}$$

where T is the temperature and K is the Boltzmann constant. As $E_{m2} > E_{m1}$, therefore $P(anti-Stokes_{m2}) < P(Stokes_{m1})$. . As compared to the m1 state, the population is less for the m2 state. Hence the probability of the anti-Stokes scattering is less than that of Stokes scattering.

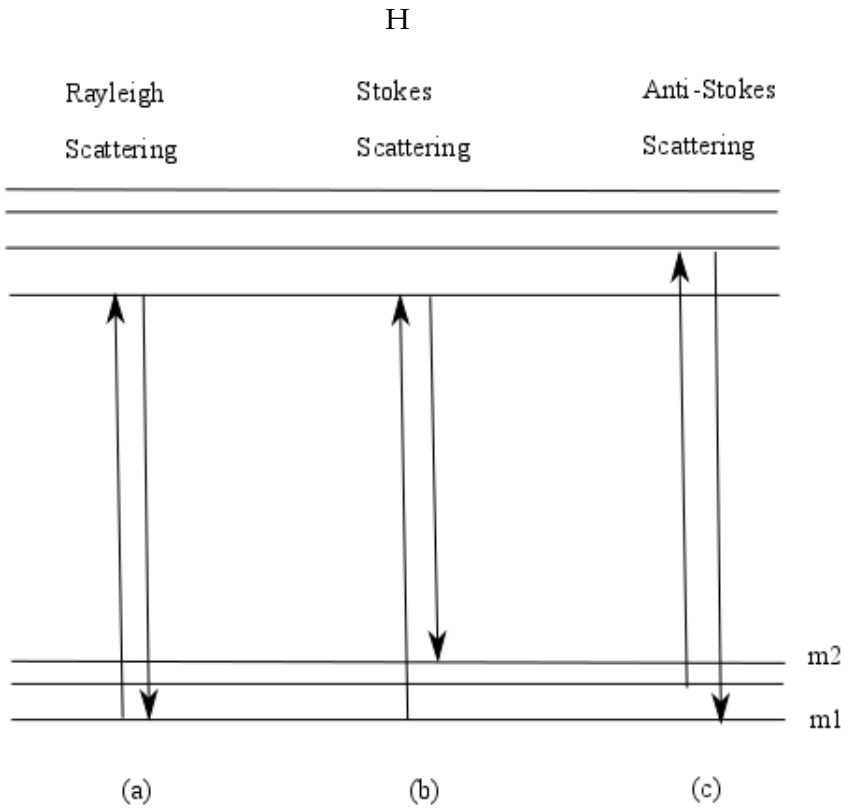

FIGURE 2.2: (a) Rayleigh Scattering (b) Stokes Scattering (c) Anti-Stokes Scattering

2.2 Polarizability Theory of Rayleigh Scattering

In this section we will get acquainted with polarizability theory of Rayleigh scattering and then apply it to Raman scattering with some pre-conditions. Polarizability is given by (2.10), where E is the applied electric field and α is a polarizability tensor. A field in one direction can induce a dipole moment in any direction. Hence α is a tensor.

$$P = \alpha E \tag{2.10}$$

$$P_x = \alpha_{xx}E_x + \alpha_{xy}E_y + \alpha_{xz}E_z \tag{2.11}$$

$$P_y = \alpha_{xy}E_x + \alpha_{yy}E_y + \alpha_{yz}E_z \tag{2.12}$$

$$P_z = \alpha_{xz}E_x + \alpha_{yz}E_y + \alpha_{zz}E_z \tag{2.13}$$

For most of the materials concerning us $\alpha_{xy} = \alpha_{yx}$, $\alpha_{zy} = \alpha_{yz}$ and $\alpha_x = \alpha_{zx}$. For isotropic elements these diagonal terms are zero.

Let's consider a electromagnetic field, traveling in the z direction with field components in the x and y direction. Lets consider a detector to be placed in this field with its normal of the surface in -z direction, allowing to detect fields in the x and y direction. We can use a polarizer to detect the intensity of the the fields in the x and y direction separately. The intensity ratio for the fields I_y and I_x for Rayleigh scattering is known as the depolarization ratio σ [8]. It is given by the (2.14).

$$\sigma = \frac{I_y}{I_x} = \frac{6\gamma^2}{45\bar{\alpha}^2 + 7\gamma^2} \tag{2.14}$$

$\bar{\alpha}$ is the mean value given by (2.15).

$$\bar{\alpha} = \frac{\alpha_{xx} + \alpha_{yy} + \alpha_{zz}}{3} \tag{2.15}$$

γ is the anisotropy parameter is given by (2.16).

$$\gamma^2 = \frac{(\alpha_{xx} - \alpha_{yy})^2 + (\alpha_{yy} - \alpha_{zz})^2 + (\alpha_{zz} - \alpha_{xx})^2 + 6(\alpha_{xy}^2 + \alpha_{yz}^2 + \alpha_{xz}^2)}{2} \tag{2.16}$$

The molecules in liquids and gases perform rotational and translational motion. Therefore, the values of α_{ij} change as the orientation of molecules change with the x, y and z axes. However $\bar{\alpha}$ and γ do not change with change in the orientation of the axes. Hence it makes sense to define the depolarization ratio in terms of $\bar{\alpha}$ and γ. In the isotropic case γ is zero. So the Rayleigh field is completely polarized. The maximum depolarization ratio we can obtain is $6/7$ in the case where $\bar{\alpha}$ is zero. However $\bar{\alpha}$ is never zero because all materials always have some positive value. So depolarization ratio is less than $6/7$. Rayleigh scattering can never vanish.

The above discussion is applicable for Rayleigh scattering. To apply this to the Raman scattering, there are certain conditions which need to fulfilled and will be discussed in next section.

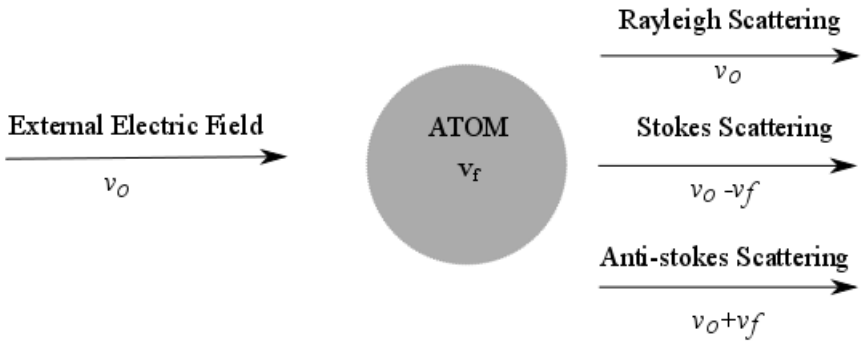

FIGURE 2.3: Interaction of an atom with external electric field

2.3 General Polarizability Theory of Raman Scattering

The general polarizability theory of Raman scattering discusses the conditions needed to be fulfilled to apply the discussion from the previous section. Let's discuss the effect of an electric field on an atom. An atom is made up of a positively charged heavy nucleus at the center with negatively charge electron cloud around it. In an unperturbed atom, the electron cloud and nucleus are performing complex vibrational and rotational motions. This complex motion is a superposition of various vibrational and rotational modes of the states of the atom. Each vibrational and rotational mode has its own polarization and frequency of vibration v_f. When a electric field of frequency v_o is superimposed on this vibration, we get fields with beat frequencies of $v_o - v_f$ (Stokes) and $v_o + v_f$ (anti-Stokes). The nucleus itself has some internal vibrational and rotational motions. These vibrations are generally in the infrared range. So for these vibrations not to interfere with the interaction of external electric field with the vibro-rotational motion of the states, the v_o and v_f must be larger than frequency of the internal vibrations and rotational frequencies of the nucleus. Hence

v_o and v_f should be in ultraviolet, visible or near infrared range. This is the first condition which needs to be fulfilled.

Second condition which needs to be fulfilled is that the ground state should be non degenerate, as the formulas developed in the previous section consider the ground state to be non-degenerate.

2.4 Placzeks Simplified Polarizability Theory

An atom has six degrees of freedom, three translational and three rotational motion. The wavefunction of these states of the atom can be described as a function of these six degrees of freedom. As described in the previous section, we can break down the complex motion of the vibrational and rotational motions into a super-position of simple vibrational and rotational motions. Each of these vibrational and rotational motions is represented by a normal co-ordinate Q. This Q is a function of six degrees of freedom. We can also represent the polarizability α in terms of Q. The polarizability α changes by a small amount with change in Q, so we can expand α as a Taylor series around an equilibrium value α_o, with higher order terms are neglected, we have

$$\alpha = \alpha_o + (\frac{\partial \alpha}{\partial_Q})_o Q \tag{2.17}$$

$(\frac{\partial \alpha}{\partial_Q})_o$ is the rate of change of α with Q near the equilibrium value. Only fundamentals are allowed as per Placzeks simplified polarizability theory. No overtones or combination tones are allowed as higher order terms of the Taylor series are neglected. We can calculate α_{nm} by (2.18).

$$\alpha_{nm} = \int \psi_n^* \alpha_o \psi_m dQ + (\frac{\partial \alpha}{\partial_Q})_o \int \psi_n^* Q \psi_m dQ \tag{2.18}$$

Let's consider the vibrations, which are represented by wavefunctions, to be a simple harmonic motion. For simple harmonic motion, the first term in (2.18) is zero unless $m = n$. The second term is zero unless $m = n \pm 1$, so α_{nm} is proportional to $(\frac{\partial \alpha}{\partial_Q})_o$ and the Raman intensity is proportional to

$(\frac{\partial\alpha}{\partial Q})_o^2$. Similar to the discussion of Rayleigh scattering in Section 2.2, we can define $\bar{\alpha}'$,γ' and σ' which are related by (2.19).

$$\sigma' = \frac{I_y}{I_x} = \frac{6\gamma'^2}{45\bar{\alpha}'^2 + 7\gamma'^2} \tag{2.19}$$

So σ' is a depolarization ratio for Raman scattering which is equal to $\frac{I_y}{I_x}$. $\bar{\alpha}'$ and σ' are the parameters for $(\frac{\partial\alpha}{\partial Q})_o$ corresponding to $\bar{\alpha}$ and σ for α. The key difference is that the Rayleigh scattering never vanishes as $\bar{\alpha}$ is never zero. However, $\bar{\alpha}'$ and γ' are derivatives, so they can be positive, negative or zero. So σ' can be zero and hence Raman scattering for that particular motion can be forbidden.

Hence, we have discussed the various theories, used to calculate the intensity for normal Raman scattering. However, these theories are incapable of explaining and calculating the intensities for resonance Raman scattering. The theory for resonance Raman scattering will be explained in the next section.

2.5 Resonance Raman Scattering (RRS)

Raman scattering is enhanced for a molecule, when the excitation frequency v_o is close or equal to the one of the energy levels (higher than the ground state). Based on this, the RRS can be classified into two types pre-resonance Raman Scattering (PRS) and rigorous resonance Raman scattering (RRRS). When v_o is close to the energy manifold but not inside the energy manifold, we call this PRS. When v_o is inside the energy band or matches any of the levels in the energy manifold, we call it RRRS. (2.5) states that intensity is proportional to $(v_o + v_{nm})^4$. In general v_{nm} is in the infrared range and v_o is in the visible or UV range. Hence, the incident frequency $v_o >> v_{nm}$ and the intensity is approximately proportional to $(v_o)^4$. The intensity is also proportional to α_{nm}^2.The quantum mechanical result for α_{nm} is given by (1.20)

$$\alpha_{nm} = \frac{1}{h}\sum_{i}^{r} \frac{\mu_{mi}\mu_{in}}{v_{im} + v_o + i\delta_r} + \frac{\mu_{ni}\mu_{im}}{v_{in} - v_o + i\delta_r} \tag{2.20}$$

where α_{nm} is the transition polarizability between the m and n states for the α operator and μ_{ni} and μ_{im} are the transition moments of the electronic dipole moment operator μ, with δ_r as the damping constant. v_{in} and v_{ir} are generally in the UV range for molecules. Hence, when v_o is in the visible range and we can consider $v_{in} > v_o$. Hence we can approximately consider the intensity to be proportional to $(v_o)^4$.

When v_o is close to one of the energy bands the factor $v_{in} - v_o$ becomes very small. Lets assume δ_r to be zero. The second component of (2.20) becomes large and we can neglect the first component, as $v_{in} + v_o$ is in the denominator. Therefore the contribution of α_{nm} becomes huge and we see an increase in the Raman intensity which is known as resonance Raman effect. The $(v_o)^4$ dependence of the Raman intensity breaks down for the RRS.

We will now define the term δ_r. Lets consider an absorption spectrum of a particular material as a function of the wavelength. An absorption spectrum may consists of peaks and valleys. $2\delta_r$ corresponds to the FWHM (full width half maximum) of the absorption peak centered at a particular wavelength.

2.5.1 Intensity Equations for RRS

The intensity for RRS, when v_o is close to the bands (PRS Case) is given by (2.21).

$$I_{nm} \propto (v - v_o)^4 \frac{(v_{eg}^2 + v_o^2)^2}{(v_{eg}^2 - v_o^2)^4} \tag{2.21}$$

where v_{eg} corresponds to the vibronic absorption maximum. This equation has been both empirically and theoretically verified.[8]

(2.21) fails to describe, however, what happens when $v_{eg} = v_o$ (RRRS case). This is where δ_r comes into picture. δ_r is never zero in the (2.20), always having some finite value. Hence, the denominator never goes to zero, having some finite value. It has been observed that, when $v_{eg} = v_o$,

I_{nm} becomes proportional to the absorption coefficient. This too has been verified empirically and theoretically.[8]

Now in the case of RRRS, the intensity also depends on the δ_r as $v_{eg} = v_o$. So the smaller the δ_r is, higher will be the Raman intensity. In the case, where $2\delta_r$ is smaller than v_{nm}, it can be shown that the generation of overtones is possible along with the fundamental. However, the intensity of the overtones depends on the absorption spectra at the overtones. So RRRS is not possible for all molecules. For a detailed discussion about the theory for RRRS please refer to paper.[9]

2.5.2 Raman scattering and Fluorescence

The Raman scattering process is an instantaneous process with a time scale of picoseconds or less. Fluorescence is a process where light is emitted due to a different process as compared to that of Raman process and its timescale is in nanoseconds. In the fluorescence process, an electron is excited to higher excited vibrational and electronic state, using an external perturbation (such as incident photon). These states are always real as compared to Raman process where they can be virtual. These excited electrons relax to lowest vibrational level of the excited state through a non-radiative process and eventually these electrons decay to the ground state by emitting a photon which is called fluorescence.

The basic three properties of fluorescence are as follows (a) fluorescence emission is Stokes shifted.(b)the absorption spectrum and fluorescence spectrum are mirror images of each other as per 'Franck Condons Principle'.(c) lastly the 'Kasha–Vavilov rule' states that the fluorescence spectrum generally shows no or little dependence on the excitation wavelength.

The process of fluorescence is completely different as compared to the Raman process and so are their spectra. Raman spectrum is unique to each molecule; fluorescence spectrum is also unique, but it does not give detailed information about the molecular structure of the material as compared to the Raman spectrum. In many molecules , the fluorescence spectra and the

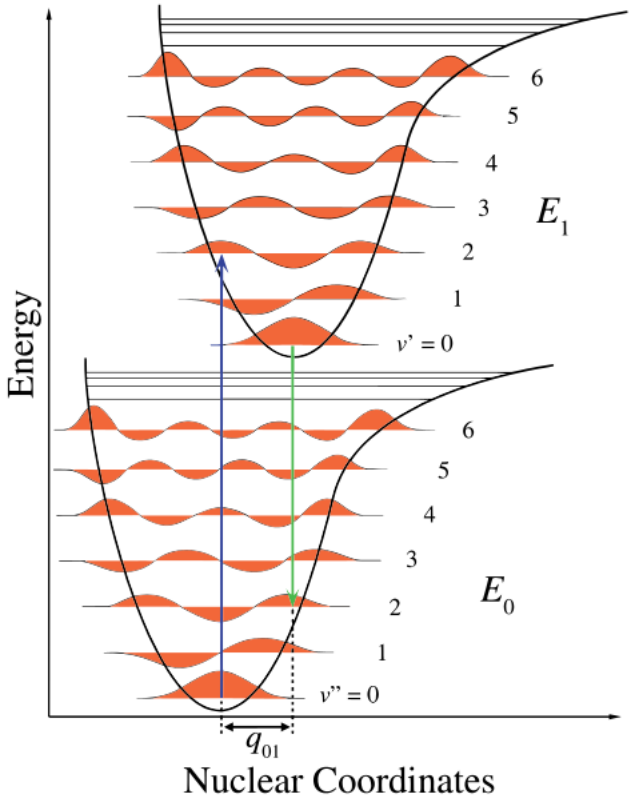

FIGURE 2.4: Raman scattering and fluorescence overlap *(Franck Condon Diagram.svg, Attribution :Samoza, wikimedia.org)*

Raman spectra overlap. Raman scattering is a weak phenomenon as compared to the fluorescence, thus the fluorescence spectrum can completely or partially mask the Raman spectra. Even for the partial masking of the Raman spectra, its hard to judge the actual intensities of the Raman peaks and hence we lose some valuable information, which can be extracted from the Raman intensities. For the research fraternity working with the Raman spectra, fluorescence is a nuisance.

Next we will discuss, the conditions under which the Raman scattering and fluorescence overlap.

Figure 2.4 shows a ground state and excited state with vibrational levels, with the energy diagram consisting of Morse potential energy curve. The highest vibrational level of the ground state does not overlap with the lowest level of excited state. Initially, the higher state corresponding to E_1 and the ground state corresponding to E_0 can be shifted from each other by q. The shift between the states depend on the molecular structure. We

consider the transition of an electron from the ground state to the excited state to be instantaneous. When an electron is excited from the ground state by an external perturbation, if the energy corresponding to v_o is not enough to excite the electron to a higher state, we will see Raman scattering with no fluorescence. When the energy is greater than the lowest level of the excited electronic state, we observe the resonance Raman effect. The shift between the states increases to q_{01}. As the electron is excited to the higher (excited) state, the excited state shifts away from the nucleus as it becomes less bounded to the nucleus. Hence, the shift between the states increases. The shift depends on the excitation frequency and the molecular structure. Now, the electrons excited to the higher vibronic levels can either undergo Raman scattering or they can relax to the lowest vibronic level of excited state, through radiation less transitions. The electrons can relax as the overlap of the wavefuntions for such radiation less transitions is large. These excited electrons, then relax to vibronic states of the ground state as per the wavefunction overlap, by emitting a photon of the corresponding energy difference. These photons correspond to fluorescence.

For the case of Raman scattering, whether the fluorescence and Raman spectra will overlap, depends on the q_{01} shift, energy difference between the levels , the energy level structure and the excitation frequency. For the first case, let's consider the q_{01} shift to be very small. The excitation frequency needs to be large enough, so that the useful Raman spectra (generally < $4500cm^{-1}$) does not overlap with the fluorescence. In second case, where the q_{01} shift is large, there is partial overlapping for the transitions of the ground states and the excited states as shown in Figure 2.4. The electrons causing fluorescence (indicated by green arrow) transit to much higher vibrational levels of the ground state. Therefore, the frequencies corresponding to fluorescence are small as compared to the first case. The excitation frequency needed to acquire fluorescence free spectra can be smaller as compared to Case 1. So there could be number of different iterations similar to the cases discussed here. But the above discussion does give a general idea of why we can get a fluorescence free Raman spectra for the

UV excitation. As UV has high frequencies, for most of the molecules, the lowest vibronic level of the excited state, is at a lower level as compared to the vibronic states contributing to the Raman effect. So the fluorescence spectra occurs at much lower frequencies as compared to the Raman spectra.

2.6 Advantages of deep UV Laser

We have developed a picosecond laser in the deep UV at 257.5 nm. Therefore, we expect to gain three advantages over conventional lasers in the visible range for the Raman measurements:

- Intensity enhancement due to higher frequency

$$I_{nm} \propto (v_o)^4 \tag{2.22}$$

- Many molecules have their bands in the deep UV, so we can get resonant enhancement
- Fluorescence free spectra for many molecules

Chapter 3

Experimental Setup

3.1 Optical Setup

The optical setup used for the Raman spectroscopy will be explained in this section. The setup shown in Figure 3.1 was used to perform the Raman measurements. A commercial 532 nm laser and a home built 257.5 nm laser were used for the Raman measurements. The dichroic filter allows all wavelengths above the laser wavelength to pass for a beam incident at 45 degrees. An objective was used to focus the light to on the sample. The sample is placed on a xyz stage (MS-2000 from Applied Scientific Instrumentation) which had resolution of 0.1 um in all 3 axes. When the sample is in focus, the objective collects the back-scattered Raman signal and directs a parallel beam of the Raman signal towards the dichroic. The dichroic filter allows the parallel beam of the Stokes Raman signal to pass and then a notch filter further filters out any residual laser beam leaking from the dichroic filter. A lens is used to focus the light onto the slit of a commercial Oriel spectrograph MS 127i. The spectrograph is coupled to a CCD camera (Andor DU-420A-BU2). The output from the camera is acquired using a custom built LABVIEW program and the program also allows the control of the xyz stage. In the following sections, we will discuss in detail the process of selection and designing the parts of the setup.

.

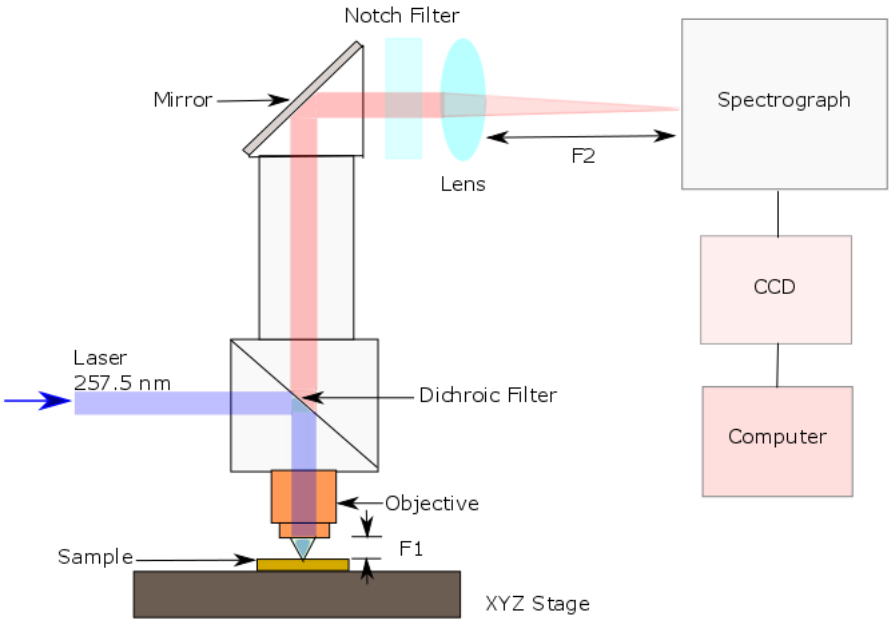

FIGURE 3.1: Raman spectroscopy setup

3.1.1 Lasers

Two lasers were used for performing Raman spectroscopy. The first laser was a commercial continuous wave 532 nm laser (Model COMPASS 315M-100). The maximum output was 100 mW. It has a polarization ratio of 100:1(vertical). The beam diameter was $@1/e^2$ 0.32 mm. The beam divergence was less than 2.2 mrad.

The second laser was a custom built laser in the deep UV at 257.5 nm wavelength with 6 picosecond pulses. The repetition rate for pulses was 60 MHz. The maximum CW power we were able to obtain was 10 mW for the setup. The beam was linearly polarized. The setup used to the generate 257.5 nm is shown in Figure 3.2. The setup was built by the graduate student Joshua Olson. I was involved in optimizing the part of the setup after the 1030 nm fiber laser output, to obtain 257.5 nm by performing second harmonic generation (SHG) twice.

The fiber setup after the pump signal combiner gave output upto 5.95 watts at 1030 nm. The iris are used to filter the central part of the diffracted beam from the fiber. A lens was used to collimate the diverging beam from

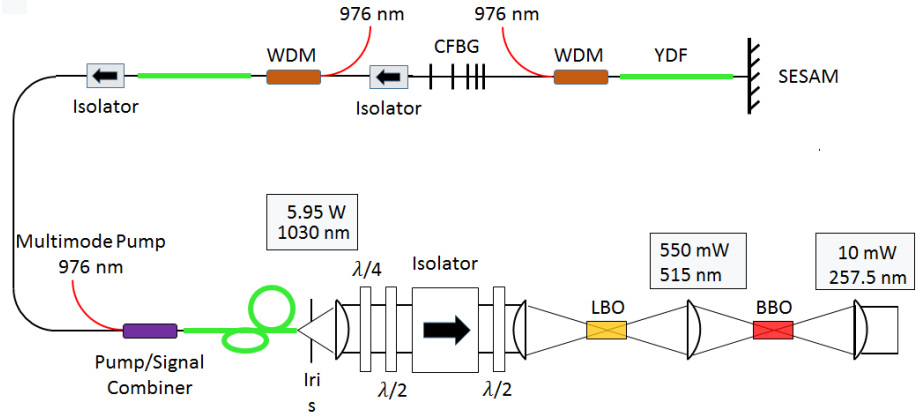

FIGURE 3.2: UV laser setup (Figure courtesy of Joshua Olson)

the fiber. The $\lambda/4$ plate (polarizer) and the $\lambda/2$ plate along with an isolator are used to set the polarization of light being focused by the lens onto a LBO crystal. The main purpose of the isolator is to prevent feedback to the fiber laser setup from reflections. The lithium triborate (LBO) crystal used in the setup is a pre-cut crystal. The optimum phase matching conditions for SHG (1030nm to 515nm) are achieved by keeping the crystal at constant temperature of $190.4°C$. The 515 nm beam was further focused onto a beta barium borate (BBO) crystal. The phase matching conditions for SHG in the BBO crystal were achieved by adjusting the orientation of the crystal on a stage with 3 translational and 3 rotational axes. The 257.5 nm beam emitted from the crystal is elliptical in shape. A cylindrical lens was used to improve the beam shape of the 257.5 nm beam. Thus a beam of 10 mW at 257.5 nm was used in deep UV Raman spectroscopy.

3.1.2 Dichroic and Notch Filters

A 532 nm stopline single-notch filter (Figure 3.3) was used as a notch filter in the Raman measurements for a 532 nm laser. A 532 nm razor edge dichroic laser-flat beamsplitter (Figure 3.4) was used as a dichroic filter. It can be seen that the transmission in the pass band is not smooth. It has

a wavy structure, with the period of the wave increasing with the wavelength. These are due to Fabry Perot effect from the finite thickness of the filters. For a filter with thickness d and refractive index n, the Fabry Perot cavity frequency spacing Δv is given by (3.1), where c is the speed of light.

$$\Delta v = \frac{c}{2nd} \tag{3.1}$$

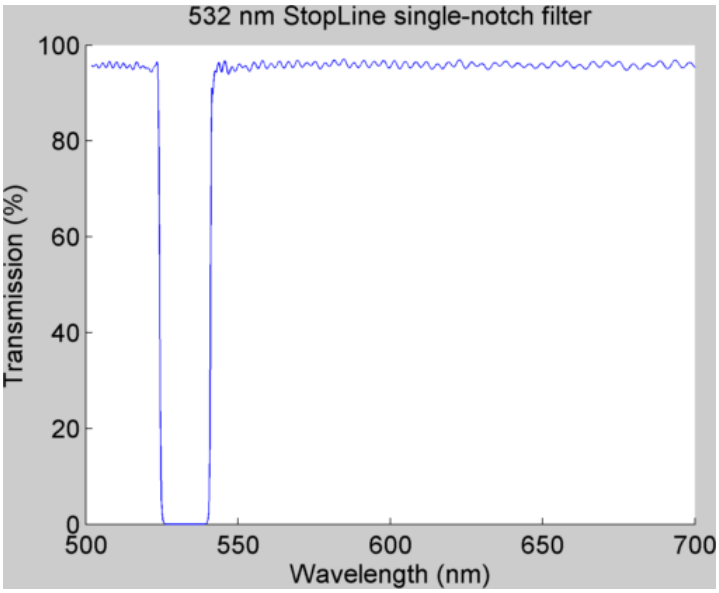

FIGURE 3.3: 532 nm stopline single-notch filter transmission

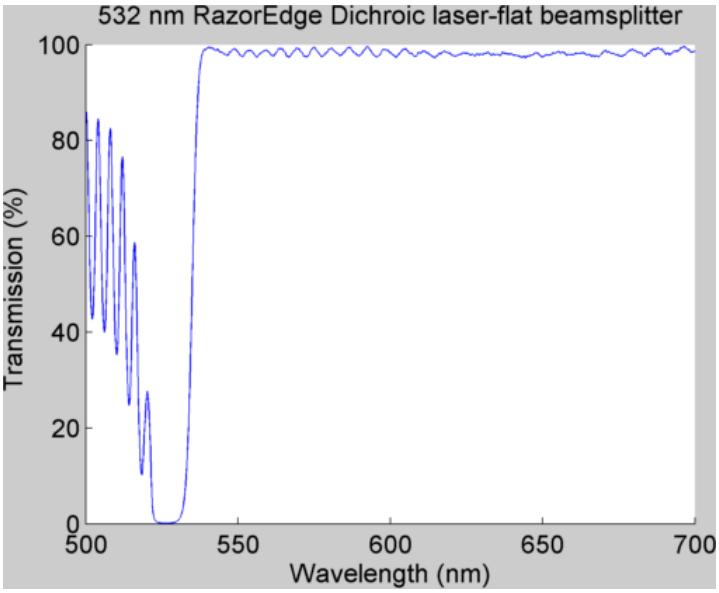

FIGURE 3.4: 532 nm razoredge dichroic laser-flat beamsplitter

The calculations for the frequency spacing were found to be correct for all the filters. The wavy structure affected all measurements and was reduced by subtracting the background measurement from all measurements.

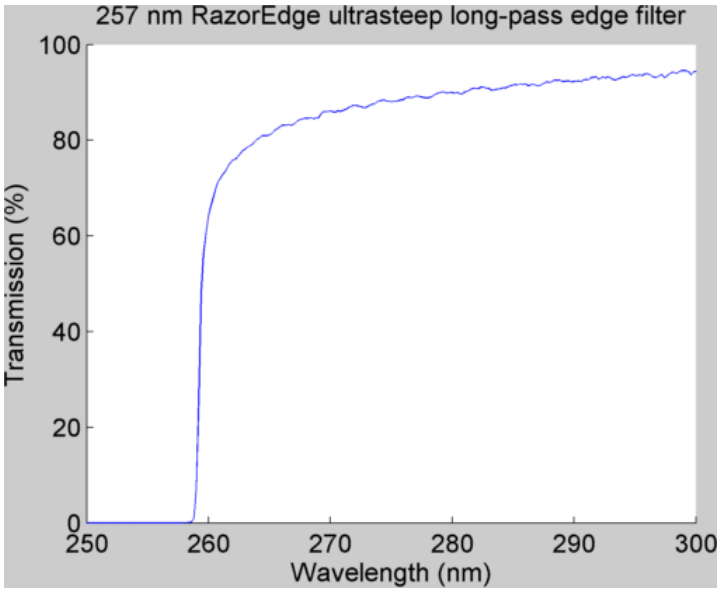

FIGURE 3.5: 257 nm razor edge ultrasteep long pass edge filter

(**For all transmissions graphs of filters, ASCII data was taken from the SEMROCK INC. https://www.semrock.com/*)

A 257 nm razor edge ultrasteep long pass edge filter (Figure 3.5) was used in place of a notch filter for the UV Raman measurements as commercial notch filters were not available. Similarly, a UV fused silica broadband precision window (uncoated) of thickness 5 mm was used in the place of a dichroic filter due to the lack of availability of the commercial dichroic filters at 257.5 nm. The transmission for parallel polarization ($r_{||}$) and perpendicular polarization ($r_{\perp}$) of light for 532 nm and 257.5 nm has been shown in Figure 3.6.

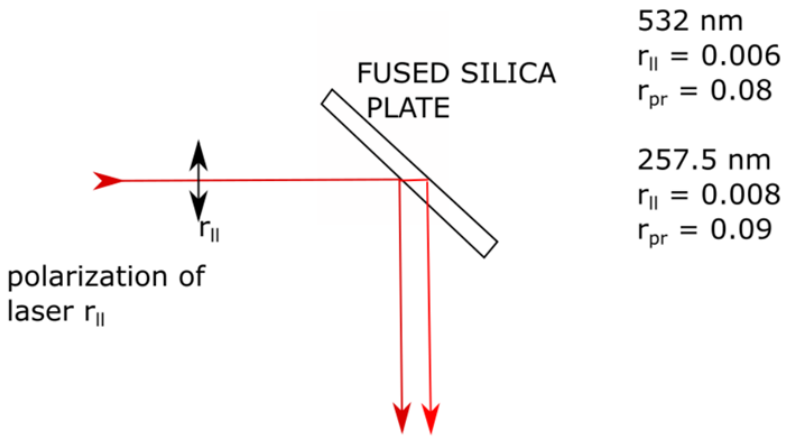

FIGURE 3.6: Fused silica plate in place of dichroic filter

Although, there are two parallel beams being reflected towards objective, only one beam can be focused through the objective. So, we can focus only 0.9 mW out of 10 mW of the 257.5 nm laser input.

3.1.3 Objective

A U-27X Newport objective was used for most of the measurements,. The objective has 27 X magnification and 0.13 NA(NA is the numerical aperture). It was used for the measurements at UV 257.5 nm and 532 nm wavelengths. The objective has a wave-front quality better than $\lambda/5$. The focal length of the objective is 4.77 mm.

The larger the NA of the objective, the smaller the spot size made by the objective. Imaging can be performed by moving the sample on the XY stage in a raster scan motion and acquiring spectra at each XY point. For an imaging system which is free of aberrations, the spot size made by an objective is given by (3.2).

$$Spotsize(radius) = 1.22\frac{\lambda}{NA} \tag{3.2}$$

For smaller wavelength the spotsize is smaller and therefore, we get better resolution. The maximum amount of Raman signal is obtained on the CCD by bringing the sample into focus by adjusting the z stage position.

3.1.4 Focusing Lens

The focusing lens was used to focus the parallel beam of the Stokes Raman signal onto the slit of the spectrograph. The focal length of the lens is 25 mm. The spectrograph has an $F/\#$ of 3.7, where $F/\#$ is the F-number (explained in the next section). For the maximum transfer of the power from the lens to the spectrograph, the $F/\#$ of both the lens and the spectrograph should be the same. If the $F/\#$ is not matching, there is loss of Raman signal due to decrease in the collimation of light. $F/\#$ for a lens is given by (3.3), where f is the focal length of the lens and D is the diameter of the beam being incident on the lens.

$$F/\# = f/D \tag{3.3}$$

The larger the focal length, the greater the $F/\#$. The diameter of the beam is equal to the back aperture of the objective which is around 6 mm for the U-27X objective. Hence, the $F/\#$ for the focusing lens is around 4.16 and is close to 3.7. To obtain $F/\#$ of 3.7, we require a lens with a focal length of 22.2 mm, but a 22.2 mm focal length lens is not available commercially and it is costly to make a custom one.

The other thing we need to take care of is that the lens is not corrected for chromatic aberrations. So the focal length for 257.5 nm is shorter than for 532 nm. Thus, the spectrometer is mounted on an XY stage and the position of the slit of the spectrometer is controlled manually to optimize the signal onto the CCD detector.

3.1.5 Spectrograph

A commercial spectrograph Oriel MS127i was used to capture the Raman spectra. The construction of the spectrograph is shown in the Figure 3.7. It uses a Czerny Turner configuration with an astigmatism correction mirror. As mentioned in the previous section, the focusing lens focuses the light onto the slit. The slit (Oriel Model 77221) width is 50 um and the height is

3 mm. The shape of the slit may result in astigmatism, if the focused point on the slit is greater than 50 um. The collimating mirror collimates the light and the astigmatism mirror corrects for astigmatism.

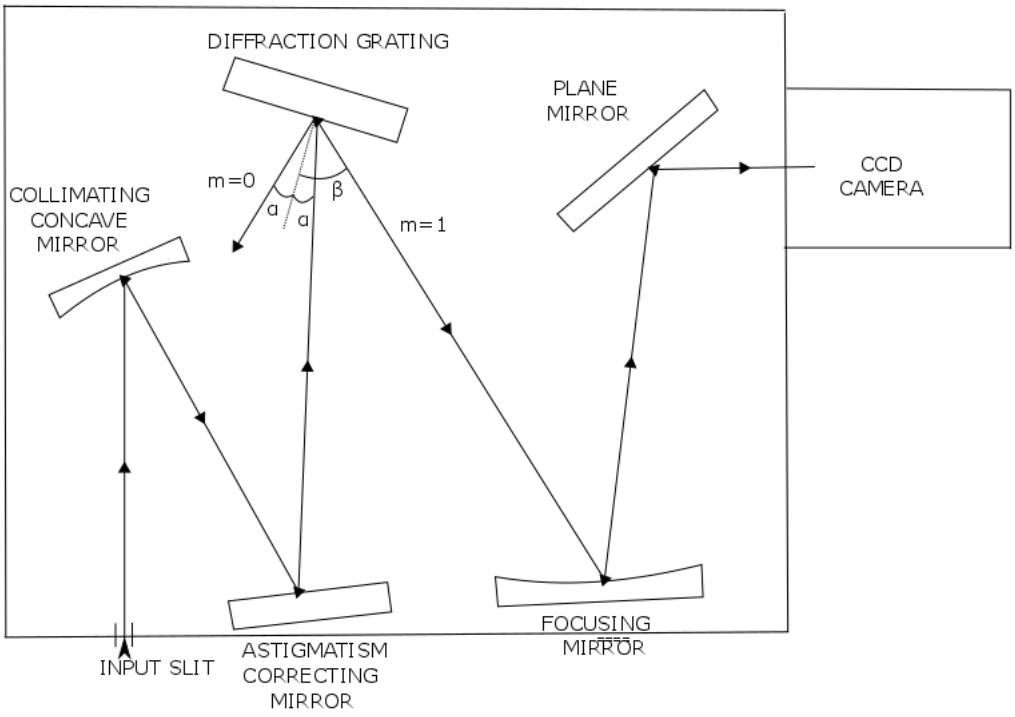

FIGURE 3.7: Construction of MS127i spectrograph

Collimated light is incident on the grating, with different wavelengths dispersed at different angles based on (3.4),

$$sin\alpha + sin\beta = mk\lambda \tag{3.4}$$

where α is the incident angle with respect to the normal to the grating, β is the diffracted angle for the wavelength λ, m is the diffraction order and k is the groove density of the diffraction grating. Each wavelength is dispersed at different angles and parallel beams of each wavelength are incident on the focusing mirror. Parallel beams at different angles to the focusing mirror form an image at different positions on the axis (CCD is along this axis) perpendicular to the optic axis.(Figure 3.8)

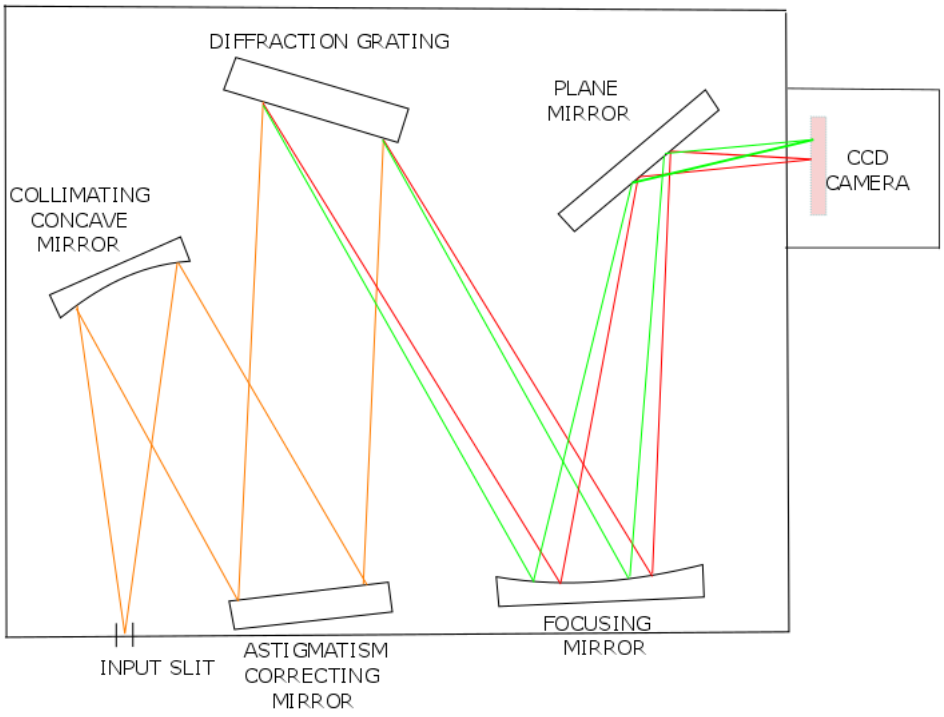

FIGURE 3.8: Image formation in a spectrograph

So in brief, the collimating mirror and the focusing mirror form an image of the slit on the CCD camera. The magnification for the configuration is given by (3.5).

$$\frac{\bar{W}}{W} = \frac{f_2 cos\alpha}{f_1 cos\beta} \tag{3.5}$$

where $\bar{W}$ is the width of the image of the slit, W is the width of the slit, f_2 and f_1 are the focal lengths of the focusing mirror and the collimating mirror, respectively. It is this equation which explains the dependence of the resolution of the spectrograph on both the slit width and the groove density of the grating. The width of the slit determines the size of the image of the slit on the CCD for each wavelength. But the distance between these images on the CCD is defined by the dispersion provided by the grating for these wavelengths. The $cos\beta$ depends on the groove density of the grating being used and the wavelength. So the magnification and hence the resolution also change with the wavelength.

3.1.6 Diffraction Grating

The diffraction grating, the slit width and the wavelength decide the bandpass of the wavelengths being focused on the CCD. The bandpass for the image of the slit width is given by (3.6).

$$Bandpass = \frac{Wcos\alpha}{mkf_1} \tag{3.6}$$

This bandpass corresponds to the image width of the slit. The total width of the band being observed on the CCD is given by (3.7).

$$Bandwidth = \frac{Bandpass * L}{\bar{W}} \tag{3.7}$$

where L is the length of the CCD. But the spectral dispersion is radial and not linear, so the value given by (3.7) is an approximation. We need calibration lamps to ascertain the actual bandwidth. The diffraction grating used for 532 nm had a groove density of 1200 gl/mm (grating lines per mm). The diffraction grating used for 257.5 nm had a groove density of 3600 gl/mm. The diffraction grating disperses different wavelengths with different efficiencies for a particular order of diffraction. The diffraction efficiency curves for the 1200 gl/mm and the 3600 gl/mm grating are given in the Figure 3.9 and 3.10 respectively. These gratings have parallel grooving lines. Therefore, different polarizations of light have different diffraction efficiencies as shown in the Figure 3.9 and 3.10. The 1200 gl/mm grating is a ruled grating. These diffraction gratings are manufactured with the use of a ruling engine by burnishing grooves with a diamond stylus. The 1200 gl/mm grating has a 500 nm blaze and a blaze angle of 17.27 degrees. For 500 nm wavelength, the reflected beam and the diffracted beam of the first order are in same directions, indirectly maximizing the efficiency at 500 nm. The wavelength 532 nm is closer to the wavelength 500 nm.

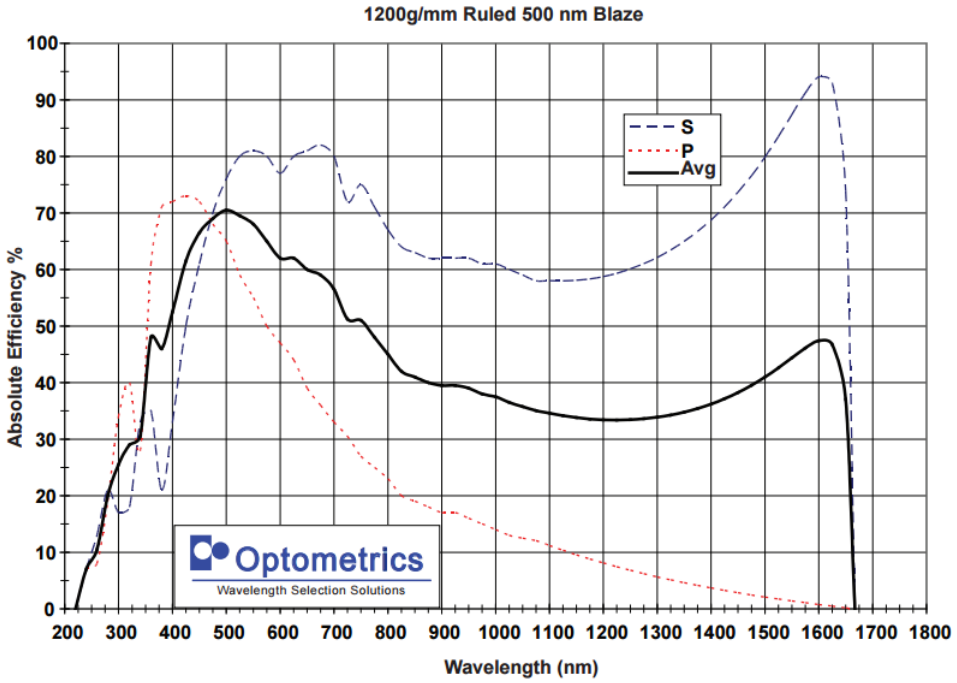

FIGURE 3.9: Diffraction efficiency of 1200 gl/mm grating

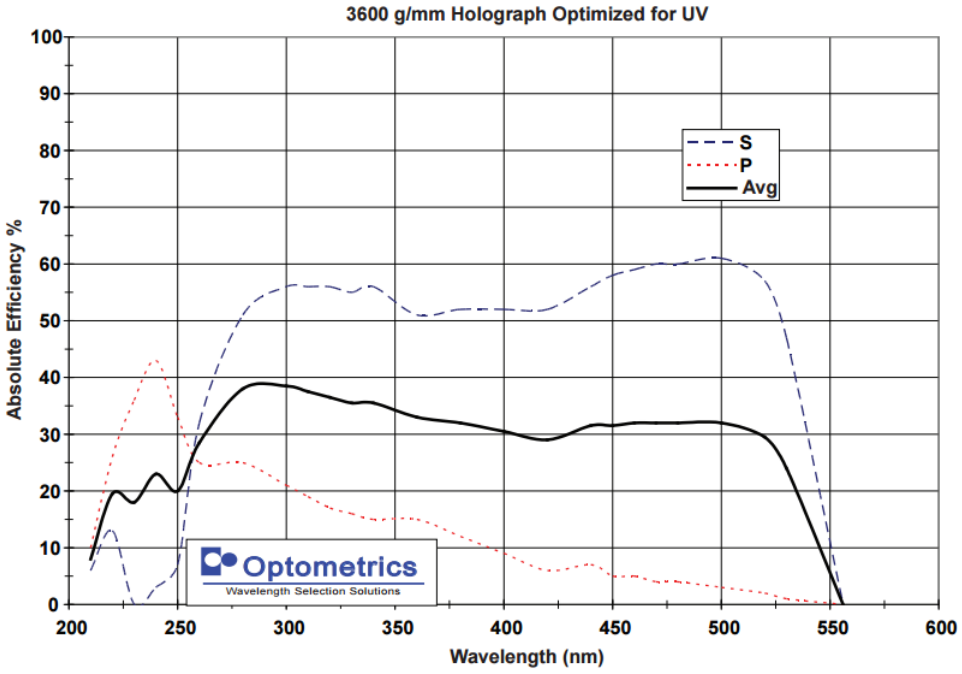

FIGURE 3.10: Diffraction efficiency of 3600 gl/mm grating

The 3600 gl/mm grating is a holographic grating. These diffraction gratings are manufactured holographically with the use of interference fringes

generated at the intersection of two laser beams.

(**Figures 3.9 and 3.10 courtesy of Optometric INC. http://www.optometrics.com/reflection-gratings)

The diffraction grating for MS 127i is fixed on a rotating stage (dial), so its position has to be manually fixed. The rotating stage has a ruled scaling on it to fix the position of the rotating stage, but there is no locking mechanism to fix it at a particular scaling value. As we rotate the diffraction grating, the bandwidth of the wavelength which is selected changes. Therefore, we need to calibrate the bandwidth for a particular fixed position of the diffraction grating.

Mercury or argon lamps were used for the calibration for the 1200 gl/mm grating. The band width comes out to be 140 nm with 590 nm as the central wavelength. For the 3600 gl/mm grating, we need zinc calibration lamp as it has some spectral lines between 250 nm and 300 nm .The bandwidth comes out to be 41 nm.

3.1.7 CCD Camera

Andor DU-420A-BU2 CCD camera was used to acquire the spectra. The BU2 series is back illuminated CCD, UV-enhanced and optimized for 250 nm. The CCD was controlled using a custom made LABVIEW program. The CCD has 1024 X 256 pixels, with a pixel size of 26 um X 26 um. The DU-420 A series can be air-cooled to -80° C. Quantum efficiency information is required for calculations in Section 4.1. All the measurements were taken at -80°C to have minimum dark current with air cooling.

(**Figures 3.11 and 3.12 courtesy of Andor Camera systems. http://www.andor.com/scientific-cameras/idus-spectroscopy-cameras/idus-420-series)

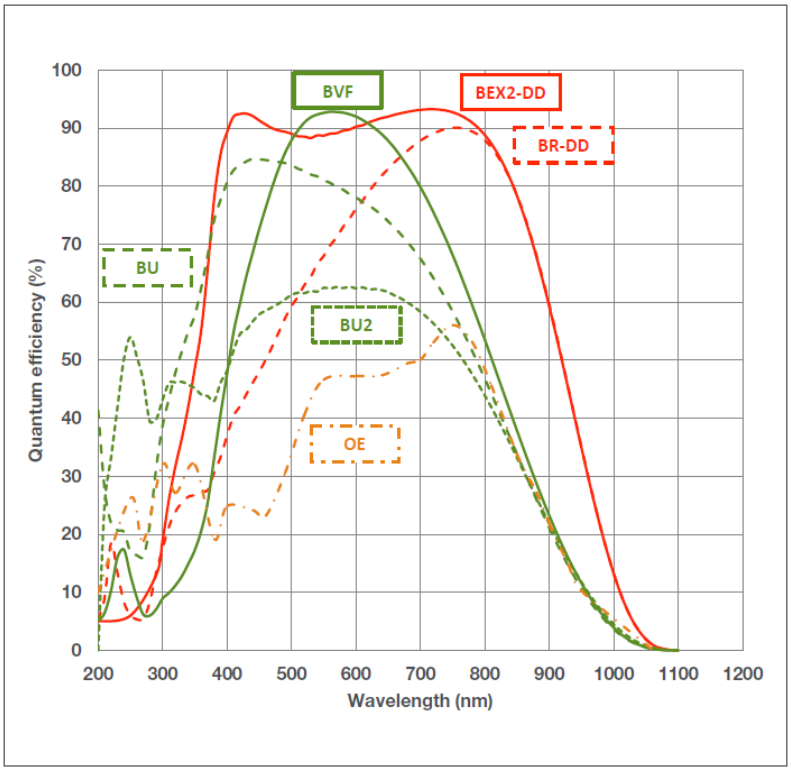

FIGURE 3.11: Quantum efficiency at -100°C

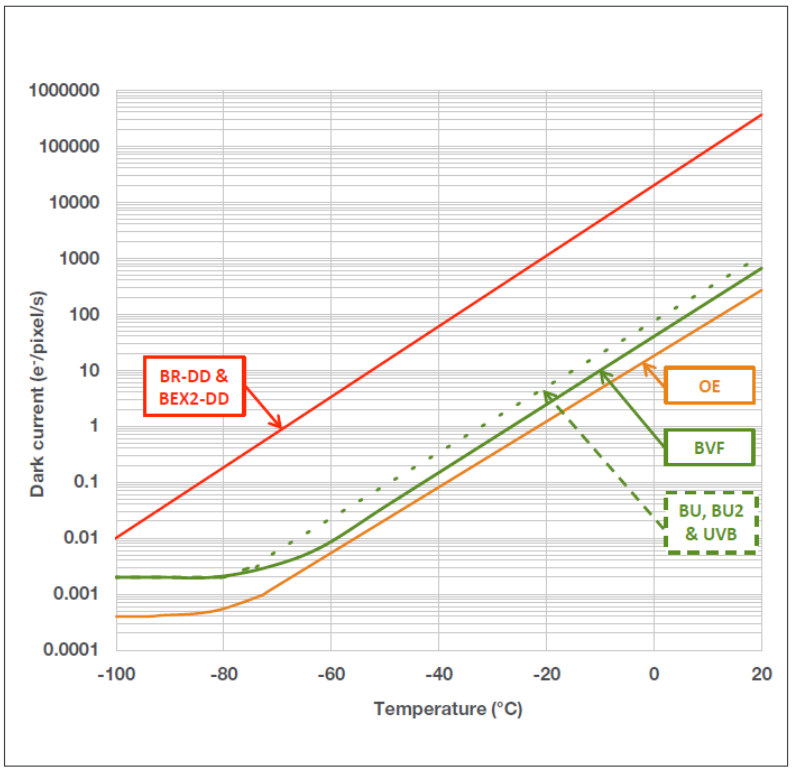

FIGURE 3.12: Dark current as a function of temperature

3.2 LABVIEW Program

LABVIEW program was used for data acquisition, image acquisition and disp1aying the image. The CCD was connected to the computer using USB 2.0. The basic drivers for communicating with the CCD camera were provided by the Andor INC, but a complete custom program was developed as per requirements.

3.2.1 Data Acquisition Program

The Figure 3.13 shows the basic program needed to acquire the spectra. The inputs for this program are temperature to which the CCD needs to cool-down, exposure time, Rayleigh wavelength, dial setting, a grating lines per mm. and blaze wavelength to select the bandwidth for particular grating. The outputs are the Raman spectra for the wavelength and the wavenumber range. The program also provides options for background correction and an option to acquire an image (not shown in picture) for specific number of X and Y pixels and resolution. The spectra are stored at each X and Y point.

3.2.2 Image Display Program

The image display program, as the name suggests, displays an image for a particular wavenumber in the spectra captured by the Data Acquisition Program. It provides for choosing a particular wavenumber and displaying the image at that particular wavenumber. It also provides for selecting a particular point in the image and displaying the whole Raman spectra acquired at that particular point. A number of image types are supported including gray, inverse gray, etc, from 6 choices. The program further allows to images be saved in different formats like jpg, tiff,etc.

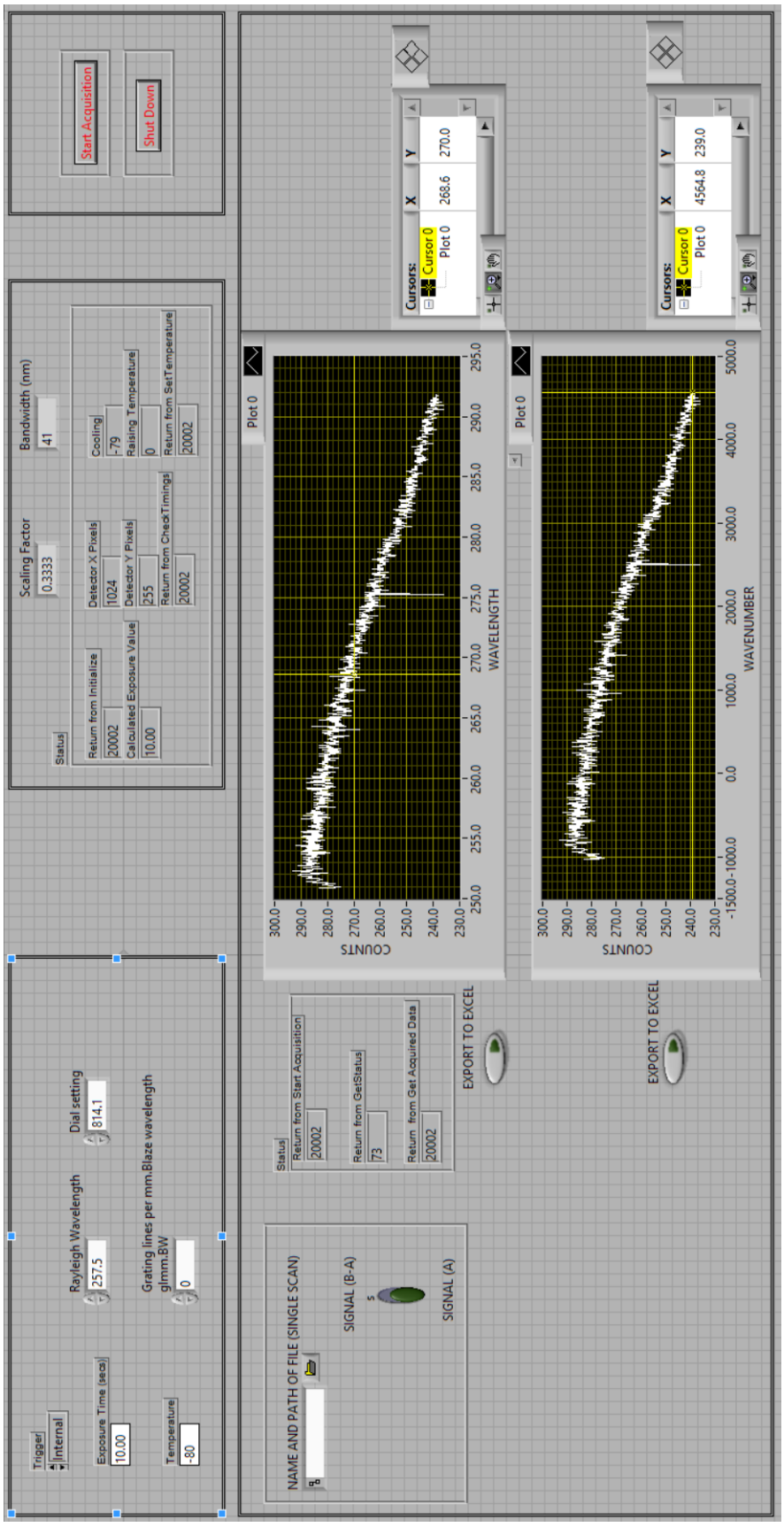

FIGURE 3.13: Labview data acquisition program (rotated)

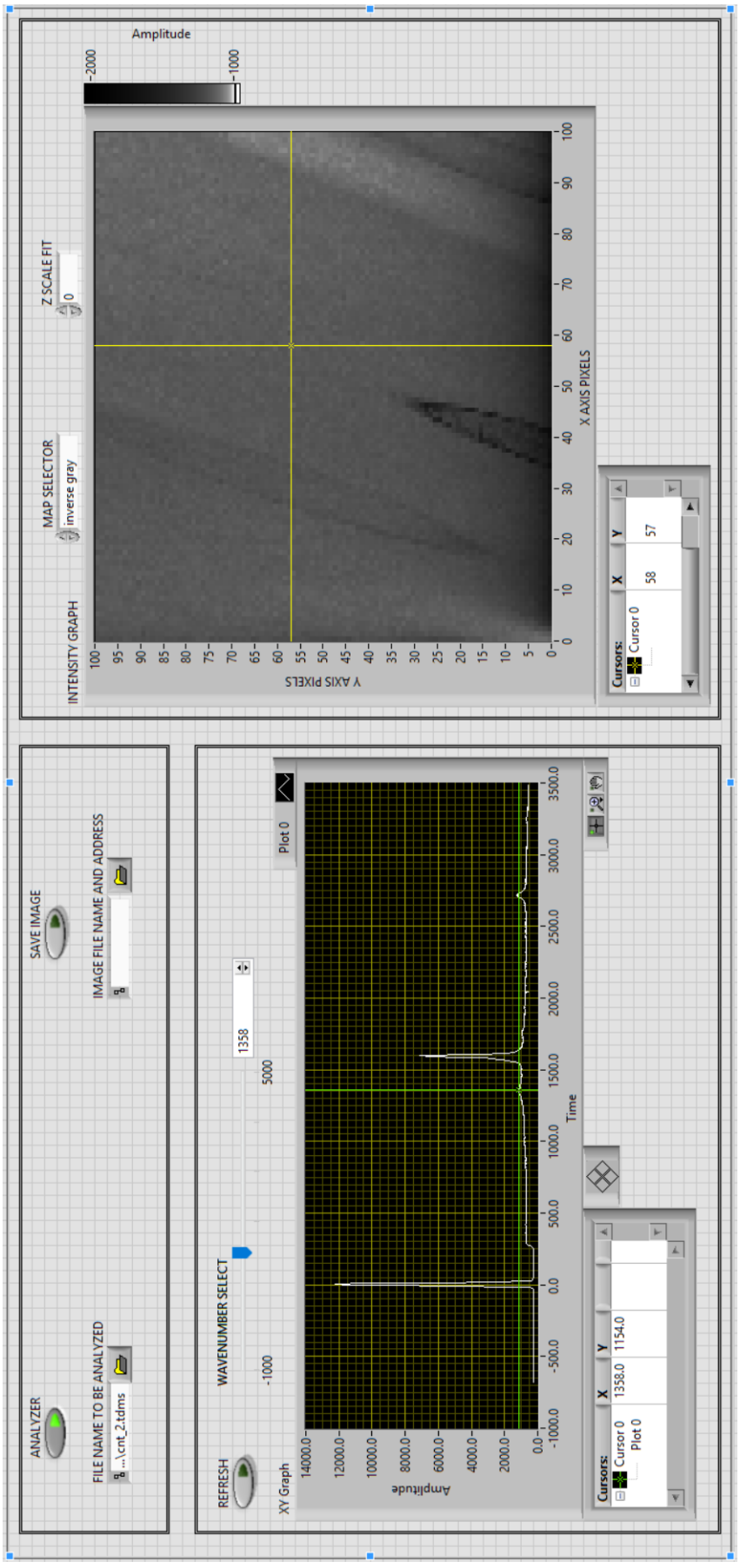

FIGURE 3.14: Labview image display program (rotated)

Chapter 4

Raman measurements and discussion

4.1 Raman spectroscopy of silicon

The Raman spectrum of a silicon sample depends on the molecular structure of the silicon. A pure silicon crystalline wafer has a strong sharp peak at 520 cm^{-1}, however, amorphous silicon has a broad peak centered at 480 cm^{-1} [10]. The compressive or tensile stress in a silicon wafer can can cause an up shift or down shift of the peak [11]. There is a wealth of research which has been done in Raman spectroscopy for different forms of silicon, but our interest was in the crystalline silicon wafer for its strong peak at 520 cm^{-1} (Figure 4.1). The peak was used as a standard for aligning the setup for 532 nm. We also verified the linear dependence of the Raman signal on the intensity of the input beam as shown in Figure 4.2. In Figure 4.1, besides the peak at 520 cm^{-1} , we observe other peaks. The peak at 0 cm^{-1} corresponds to the leaked pump laser. The other peaks corresponds to silicon dioxide (SiO_2) due to the slow oxidation of silicon.

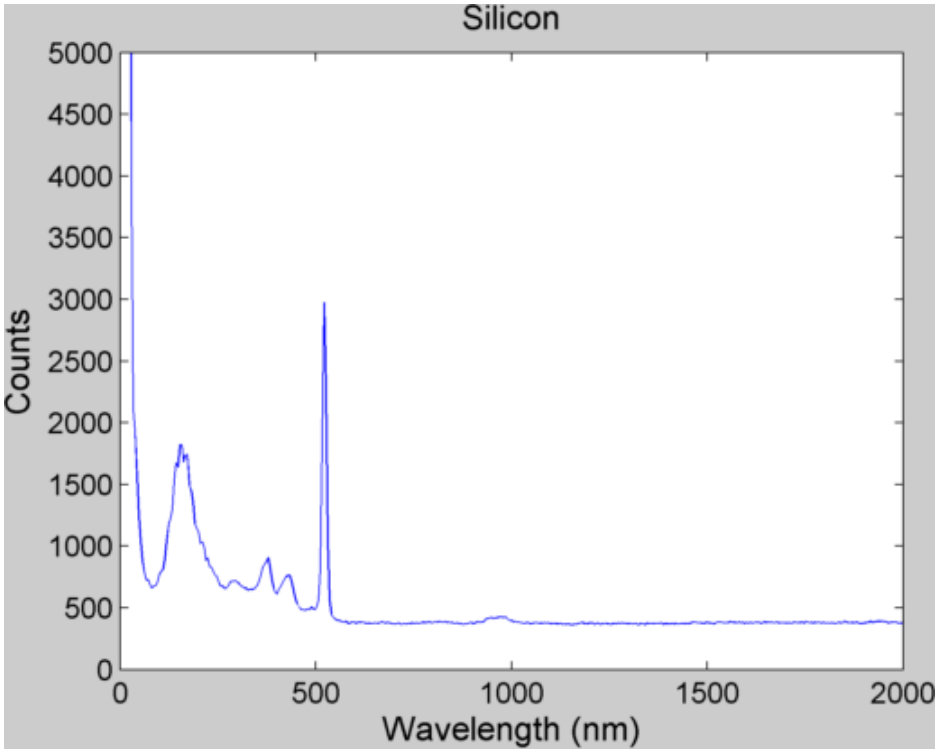

FIGURE 4.1: Raman spectrum of silicon

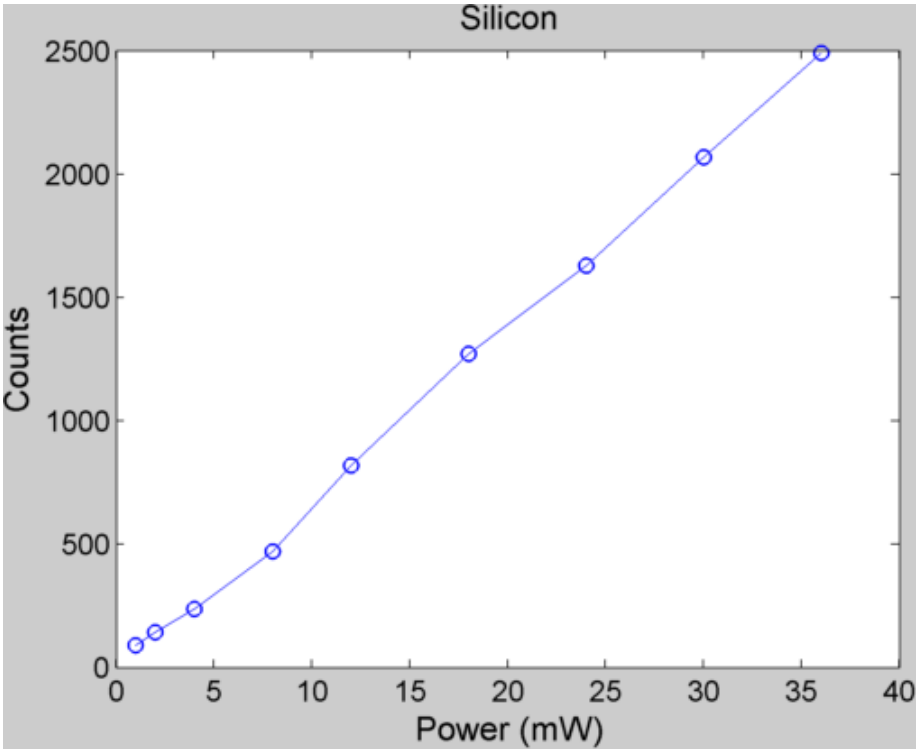

FIGURE 4.2: Linear dependence of Raman intensity versus input power

The Y axis in Figure 4.1 and 4.2 is counts, which is proportional to the intensity. All the measurements had an exposure time of 1 second.

4.2 Raman spectroscopy of water

The Raman spectrum of the distilled water was used as a standard with the 257.5 nm laser for aligning the setup. The Raman spectrum of the distilled water has a wide band between 2800 cm^{-1} and 3800 cm^{-1} corresponding to OH stretching modes. A water molecule will have only two peaks one for the symmetric stretching of OH bonds at 3657 cm^{-1} and the other for the anti-symmetric stretching at 3755 cm^{-1}. However, we are acquiring the Raman spectrum of the bulk water. In bulk water, there is a weak bonding between the water molecules, resulting in a wide Raman spectrum [12]. The Raman spectra in Figure 4.3 and 4.4 were acquired for an exposure time of 10 seconds with 550 μW power at 257.5 nm.

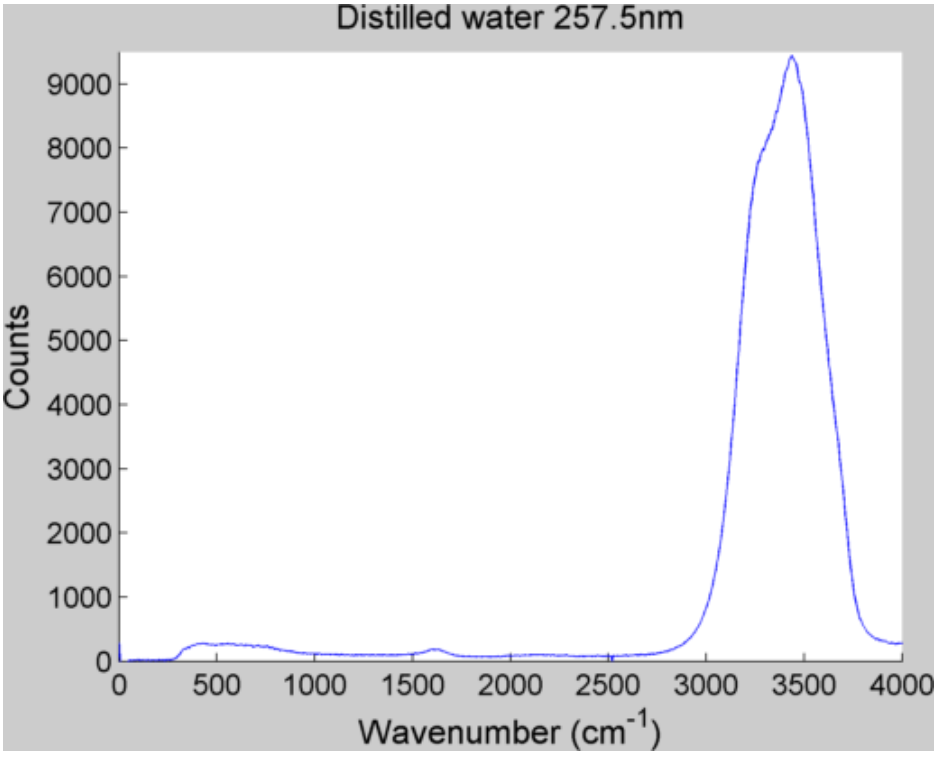

FIGURE 4.3: Raman spectrum of distilled water

For a water molecule, there would have been a single Raman peak at 1595 cm^{-1} corresponding to $H-O-H$ bending. Due to the bulk nature of water, the peak broadens and consist of two overlapping peaks one at 1640 cm^{-1} for a water molecule bonded to four other water molecules by

weak hydrogen bonds and 1580 cm^{-1} for a partially hydrogen bonded water molecule.

The band between 300 to 1000 cm^{-1} in Figure 4.4 consists of a three wide bands corresponding to the librational modes wagging, twisting and rocking, centered at 430, 650 and 795 cm^{-1} respectively.

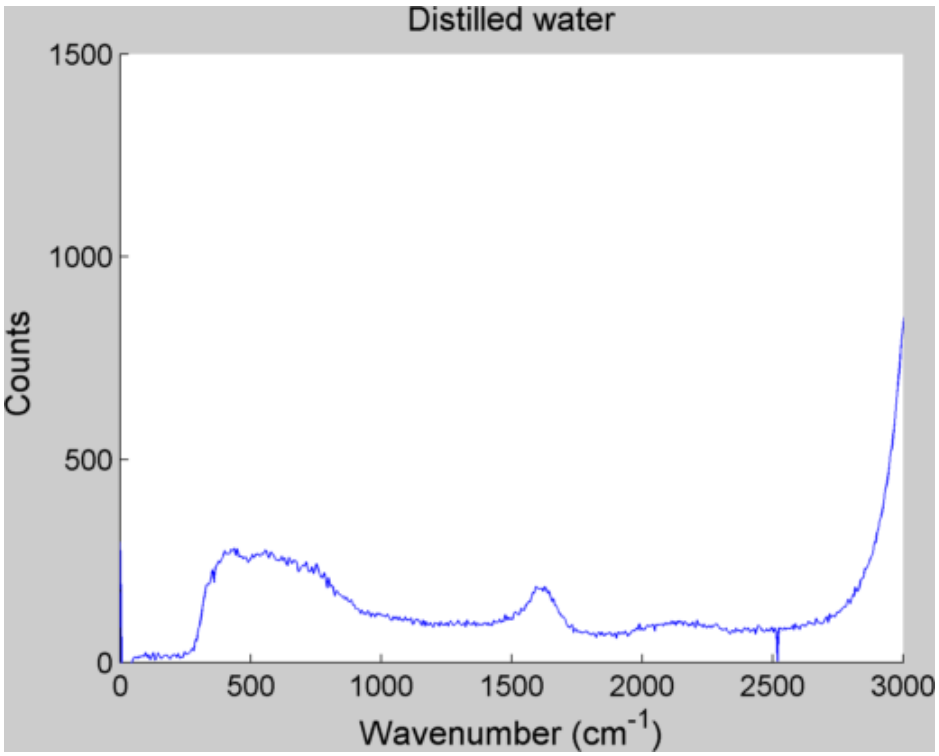

FIGURE 4.4: Raman spectrum of distilled Water

The bands corresponding to the translational modes between 65 and 162 cm^{-1} are absent due to the filter cutoff [13].

4.3 Effect on OH stretching modes in sodium sulfate solution

The idea here is to introduce the difference between the bond polarity and bond polarizability and then describe their approximate relationship and how that influences Raman intensities. The bond polarity for an X-Y molecule with a single bond is the difference in the charges between them. For an X-Y molecule with X=Y, the bond polarity will be zero. On the other hand, the bond polarizability is the ability of the molecule to get polarized on the

application of an external field. In other words, when an external electric field is applied, the electron cloud of the molecule gets distorted. The ease of the distortion is defined as the polarizability. Raman intensity is proportional to the square of the polarizability derivative with respect to the space co-ordinates as per Placzek's simplified theory.

In Figure 4.5, you can see the comparison of the Raman spectra of a 1.85 M (Molar Solution) $Na_2SO_4 + H_2O$ (red) with H_2O (blue) in the range between 2800 to 3800 cm^{-1}. Both of the spectra were acquired for an exposure time of 10 seconds with 550 μW power at 257.5 nm.

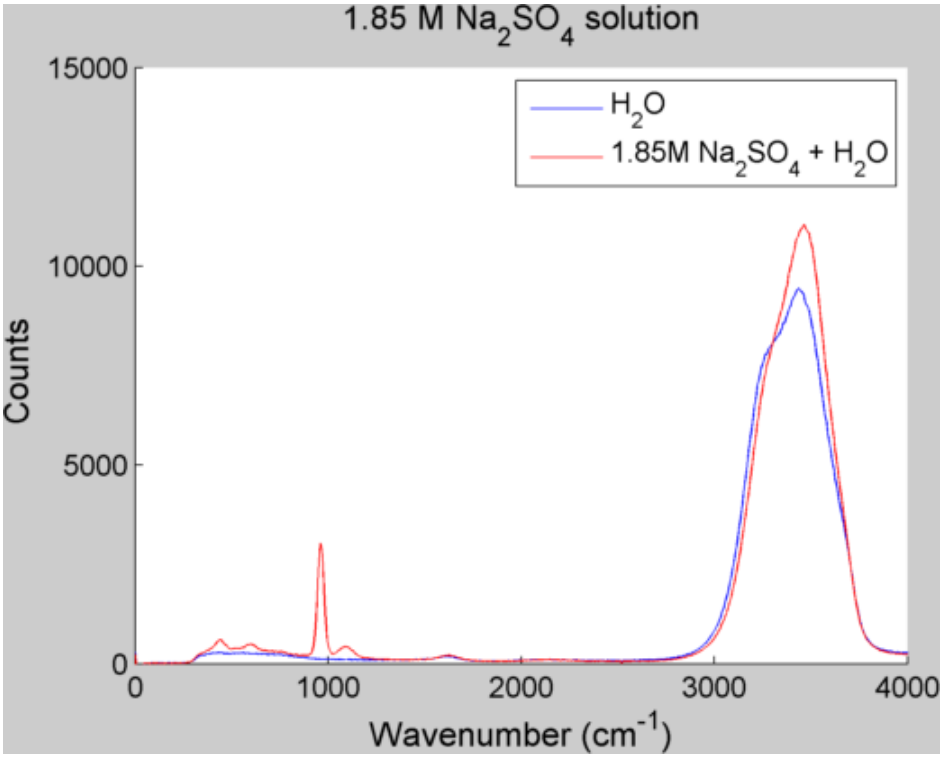

FIGURE 4.5: Raman spectrum of 1.85 M $Na_2SO_4 + H_2O$

The peak around 3500 cm^{-1} is stronger for the Na_2SO_4 solution as compared to that of the water. The peak corresponds to the weak intermolecular bonding. In bulk water, it corresponds to the $O - H - -O$ bonding between two water molecules. This weak bonding is present due to the partial positive and negative charges on the H and O atoms of a water molecule. Similarly, in the Na_2SO_4 solution, we observe a weak bonding between the double bonded oxygen atom bonded to sulfur and the $O - H$ bond of the water. However, the polarizability for the $O - H - -O$ in

Na_2SO_4 solution is greater than in H_2O. Therefore, the Na_2SO_4 solution has a stronger Raman peak at 3500 cm_{-1}[13].

The reason behind the polarizability being higher in the Na_2SO_4 solution, can be explained in terms of the bond polarity. In general, the more polar the bond is, lower the polarizability. The oxygen atom double bonded to the sulfur atom is less electronegative as compared to the oxygen atom bonded to two hydrogen atoms. The hydrogen atom has an electronegativity of 2.2 as compared to that of 2.58 for the sulfur atom. Hence, the oxygen atom bonded to the sulfur atom is less polar as compared to the oxygen atom bonded to the hydrogen atom.

Lastly, the four Raman peaks between 250 cm^{-1} and 1250 cm^{-1} for the Na_2SO_4 solution are the characteristic Raman peaks of Na_2SO_4 salt.

4.4 Raman spectroscopy of carbon nanotubes (CNTs)

The Raman spectra of the CNTs can be used to probe the properties of the CNTs, which are grown in different environment with different parameters. The generalized Raman spectrum for CNTs has been shown in Figure 4.6.

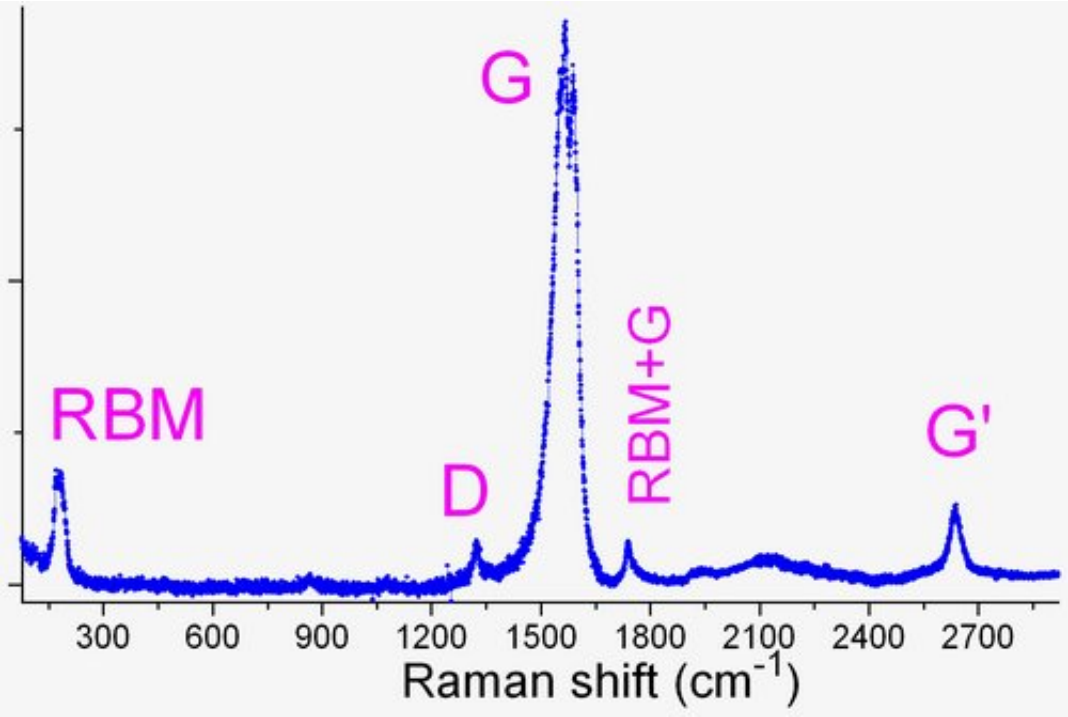

FIGURE 4.6: Generalised Raman spectrum of CNTs

The radial breathing mode (RBM) corresponds to the radial expansion-contraction of the CNTs. Therefore, its frequency v_{RBM} cm^{-1} depends on the diameter of the CNTs. The RBM range is between 100–350 cm^{-1}. Unfortunately, we cannot measure the RBM band, as the filter cutoff is at 300 cm^{-1}. If the RBM intensity is particularly strong, its weak second overtone can be observed at the double frequency.

The G mode (G for graphite) corresponds to the planar vibrations of the carbon atoms. The G band in SWCNTs (single walled carbon nanotubes) is shifted to lower frequencies relative to the graphite at 1580 cm^{-1} and gets split into several peaks. For the SWCNTs probed in this thesis, they split into two peaks. The G^+ peak corresponds to the planar vibrations parallel to the length of the CNTs. The G^- peak corresponds to the planar vibrations perpendicular to length of the CNTs.

The D mode originates from structural defects or misalignment in the CNTs. Therefore, the ratio of the G/D modes is used to determine the structural quality of the CNTs. High-quality CNTs have a ratio higher than 100.

The name of the G' mode is misleading. It is given to this mode, as it is the second strongest peak after the G mode. However, it is actually the second overtone of the D mode. Its intensity is stronger than that of the D mode due to different selection rules for the Raman intensity. The peak at 1750 cm^{-1} is an overtone corresponding to the combination of the RBM+G mode. [14]

The CNT samples used for the measurements were fabricated by REU student Lisa J. Willis under the guidance of Dr. Palash Gangopadhyay. A polymer composite was synthesized using polymethylmethacrylate (PMMA) and CNTs, with 2 percent by weight. Then a plasticizer was added during the film fabrication so that the composite can be melted at relatively low temperature. The CNTs were then aligned horizontally, vertically and 45 degrees using a magnetic field. The samples were tested using absorption spectroscopy, surface resistivity measurements, electrostatic force microscopy and polarized Raman spectroscopy, to compare their compositions, electrical properties and to investigate the efficiency of magnetic field

poling on each type of CNT.

The Figure 4.7 shows the Raman spectrum obtained for the horizontally aligned SWCNTs with all the typical Raman peaks.

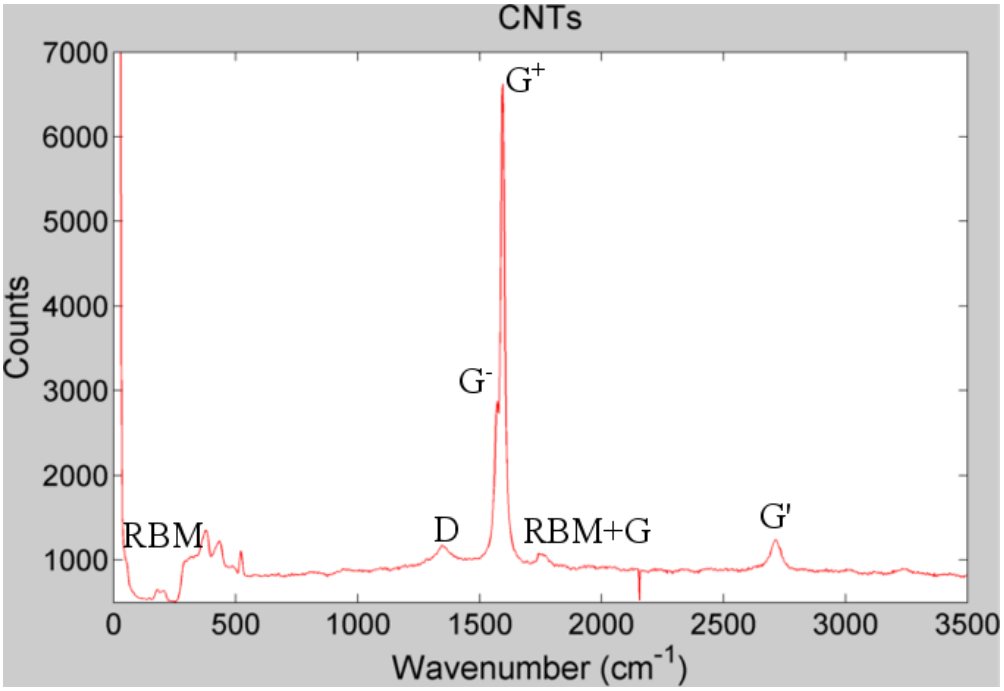

FIGURE 4.7: Raman spectrum of SWCNTs (532 nm)

4.5 Raman Spectra and Fluorescence of biological Samples

The Raman spectra for biological samples in the visible and near infrared wavelength range is generally masked by fluorescence. However, it has been observed that in the deep UV for many bio molecules, the useful Raman spectra are generally free from fluorescence. The degree of the fluorescence masking does vary for different bio-molecules.

We investigated the Raman spectra of an oak tree leaf and lactobacillus acidophilus and bifidobacteria from a probiotic medicinal capsules. We investigated two samples as a proof of concept and did not go deep into the implications of the spectra observed for each case. But in the future, we do plan to research the implications of the observed Raman spectra. We also measured the spectrum for toluene which showed a large fluorescence

at 257.5 nm and negligible at 532 nm. Toluene shows completely opposite behavior as compared to fluorescence of the bio-molecules.

The 257.5 nm laser has the shortcoming of having a 0.4 nm FWHM. The 0.4 nm FWHM translates to 60 cm^{-1} in wavenumber. In order to resolve the two peaks by the Rayleigh criterion, the maximum of one peak should be at the minimum of the other peak, hence, approximately, they should be separated by 120 cm^{-1}. To get better resolution, we need to work on getting a narrower bandwidth for the laser, buy a grating of higher groove density or design a new custom spectrometer. Secondly, we need to acquire a dichroic filter for 257.5 nm or increase the output of the laser, so that there is more incident power on the sample to get a better signal to noise ratio.

4.5.1 Oak Tree Leaf

The spectrum for 532 nm was taken at 2.7 mW for 10 seconds. The spectrum for 257.5 nm was taken at 550 μW for 60 seconds. For the Raman spectrum with 532 nm, we can see 3 Raman peaks at the top of the fluorescence for the oak leaf. The fluorescence increases with the wavenumber and rapidly increases after 2500 cm^{-1} and hence, we cannot see any Raman bands at higher wavenumbers. However, the Raman spectrum acquired at 257.5 nm (Figure 4.9) is free of fluorescence. The highest peak at 1585 cm^{-1} corresponds to trytophan and tyrosine. The second feature around 1400 cm^{-1} is pretty broad. Due to lack of resolution, the other peaks in the broad feature are not resolvable. The broad feature encompasses many peaks [15] corresponding to the different chemical constituents. The peak in the broad band corresponds to carotenoid 1279 cm^{-1} and tryptophan (indole ring) 1360 cm^{-1}.

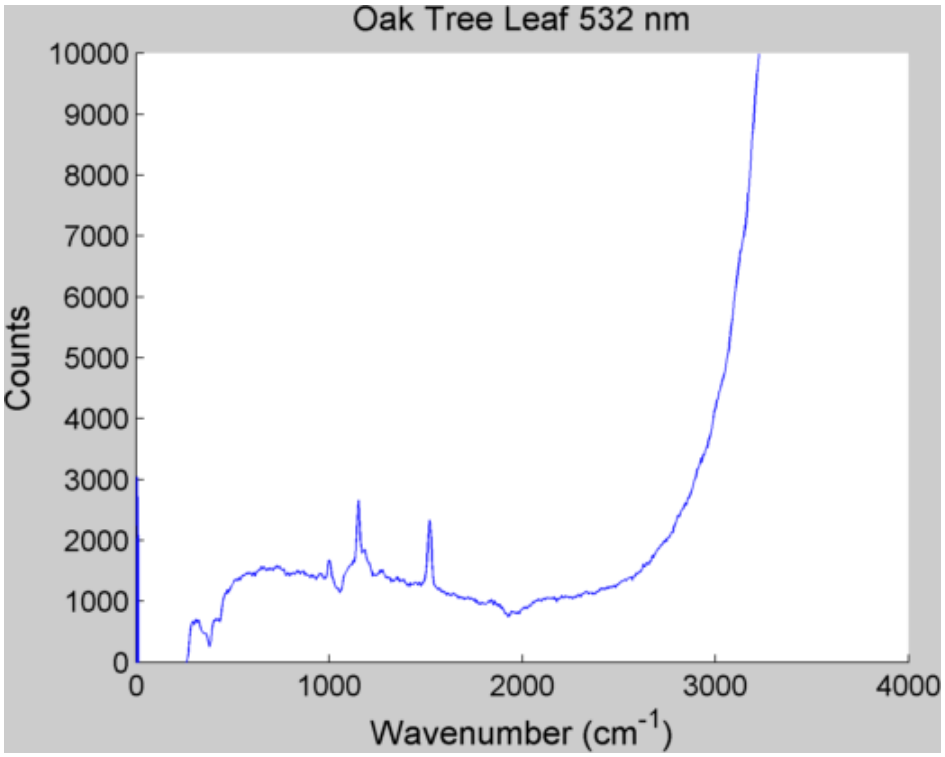

FIGURE 4.8: Raman spectrum of oak leaf with 532 nm

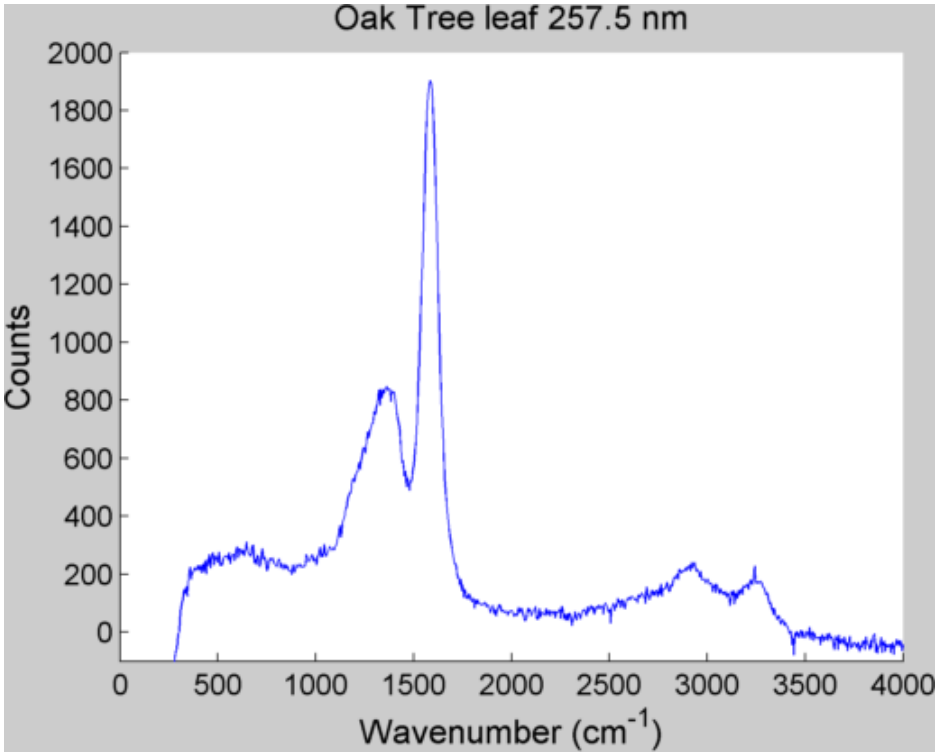

FIGURE 4.9: Raman spectrum of oak leaf with 257.5 nm

4.5.2 Lactobacillus Acidophilus and Bifidobacteria from a probotioc medicinal Capsules

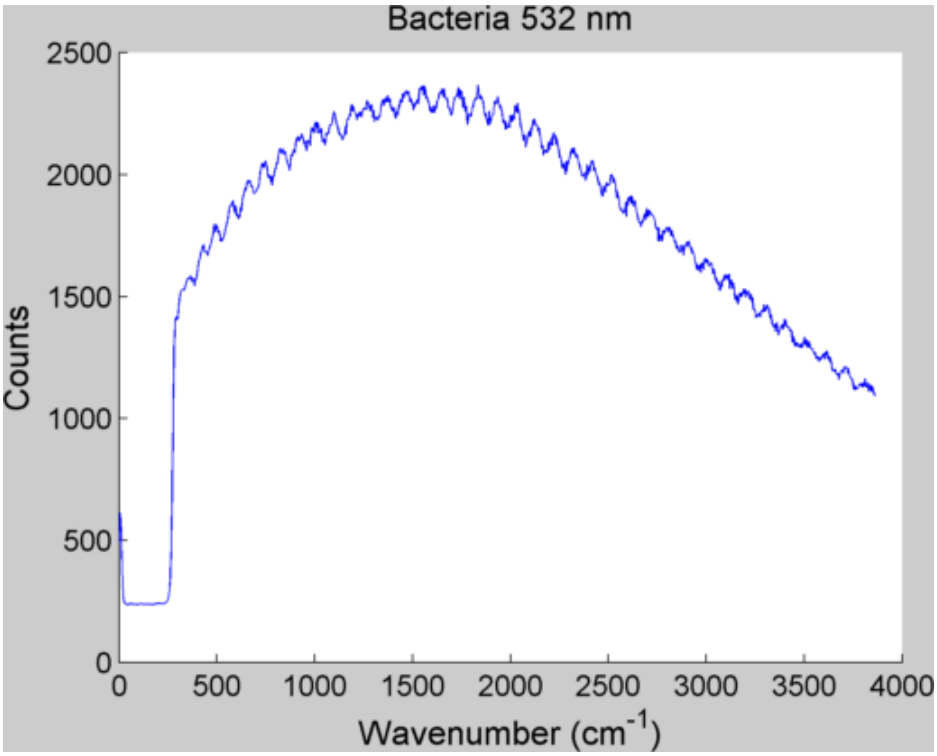

FIGURE 4.10: Raman spectrum of bacteria with 532 nm

The spectrum for 532 nm was taken at 2.7 mW for 10 seconds. The spectrum for 257.5 nm was taken at 550 μW for 60 seconds. The Raman spectrum is observed only in the UV. The fluorescence is observed for 532 nm. The peak around 1600 cm^{-1} can be assigned to the aromatic amino acids tyrosine and tryptophan. The peak around 1480 cm^{-1} can be attributed to guanine and adenine and they also contribute to the peak at 1325 cm^{-1}. The spectrum should consist of many additional peaks [16], but these are lost due to the lack of resolution.

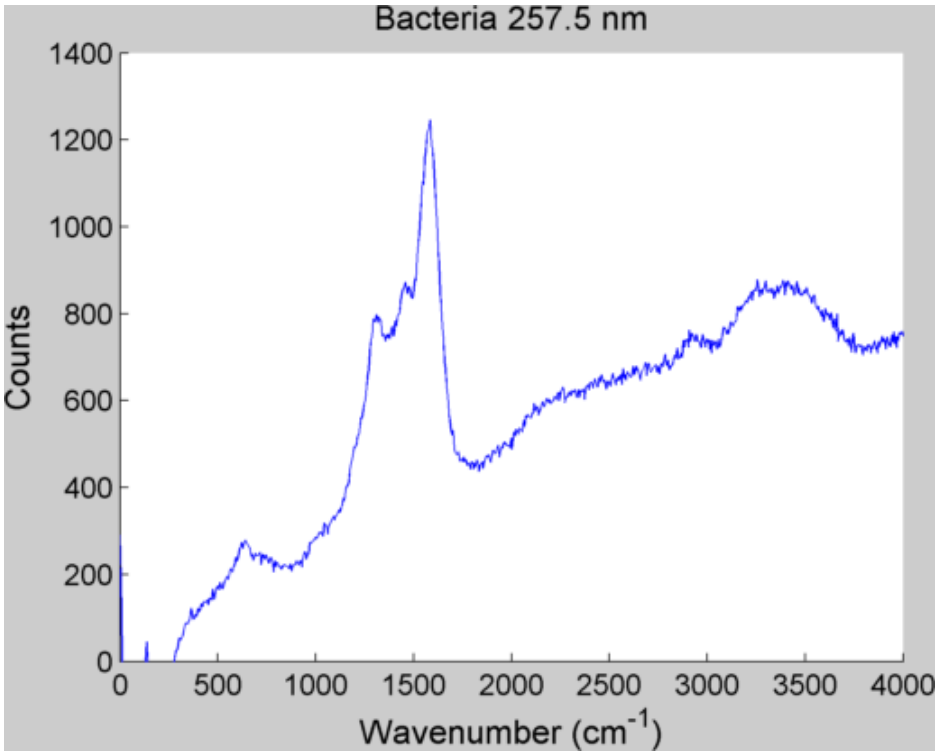

FIGURE 4.11: Raman spectrum of bacteria with 257.5 nm

4.6 Toluene

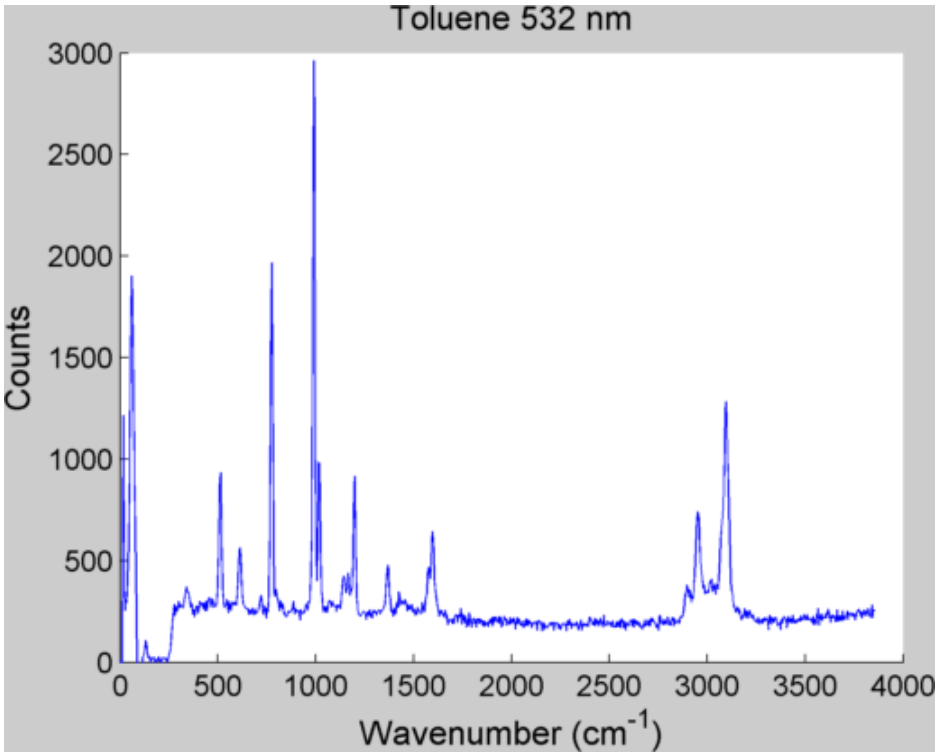

FIGURE 4.12: Raman spectrum of toluene with 532 nm

For toluene we can see the standard Raman spectrum for 532 nm but only fluorescence with 257.5 nm.

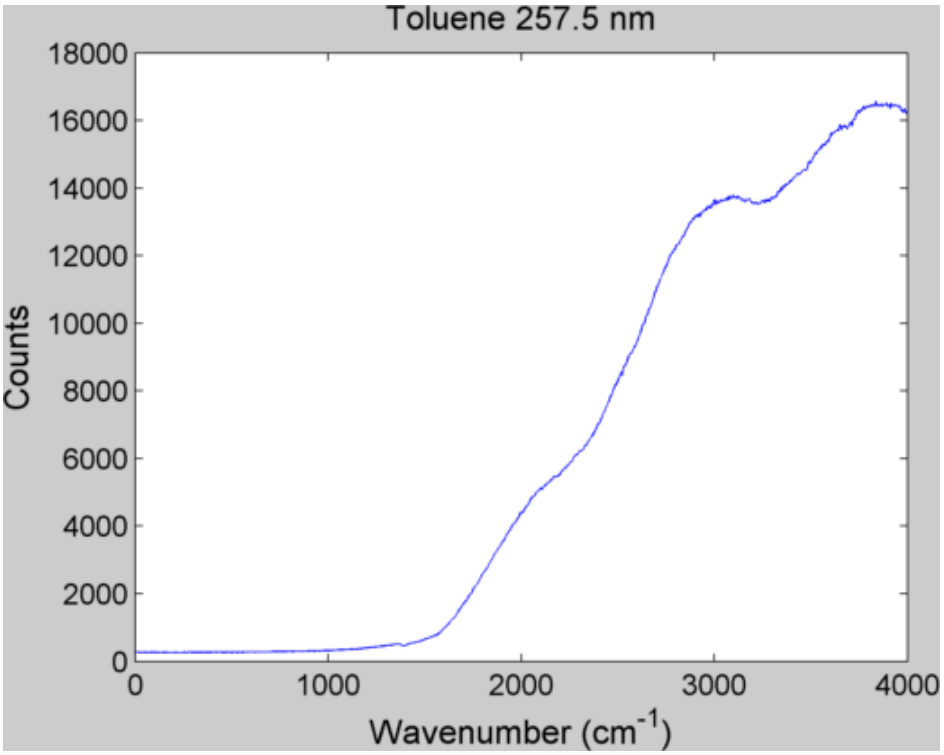

FIGURE 4.13: Raman spectrum of toluene with 257.5 nm

4.7 Resonance Raman Measurements for sodium nitrate ($NaNO_3$)

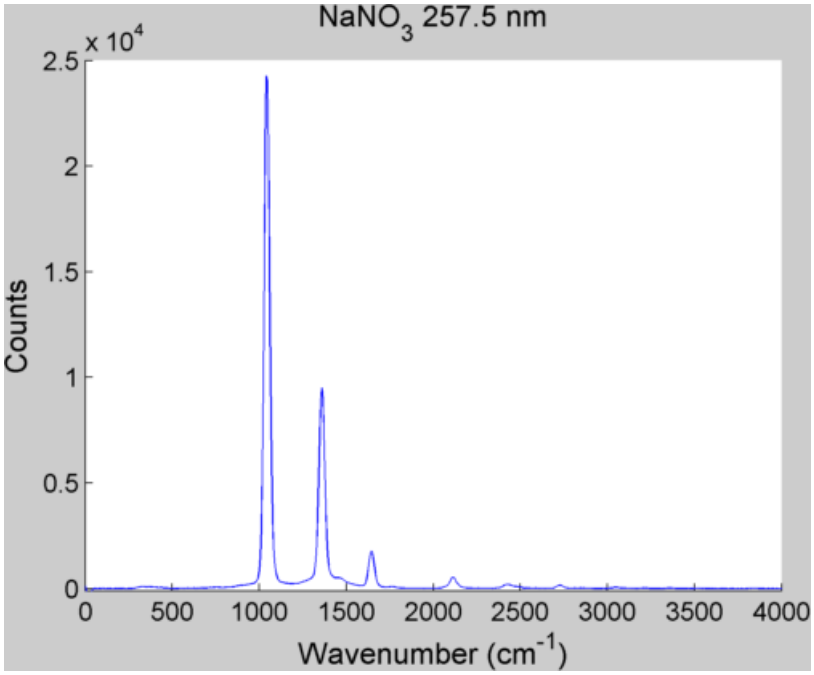

FIGURE 4.14: Raman spectrum of $NaNO_3$ 257.5 nm

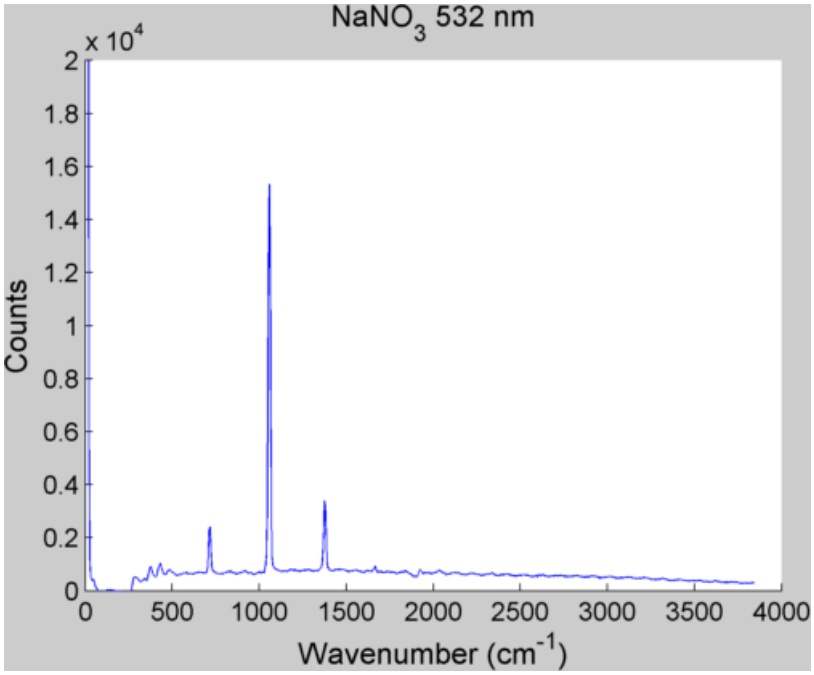

FIGURE 4.15: Raman spectrum of $NaNO_3$ 532 nm

The spectrum for 257.5 nm was taken at 550 μW for 10 seconds. The spectrum for 532 nm was taken at 2.7 mW for 10 seconds.

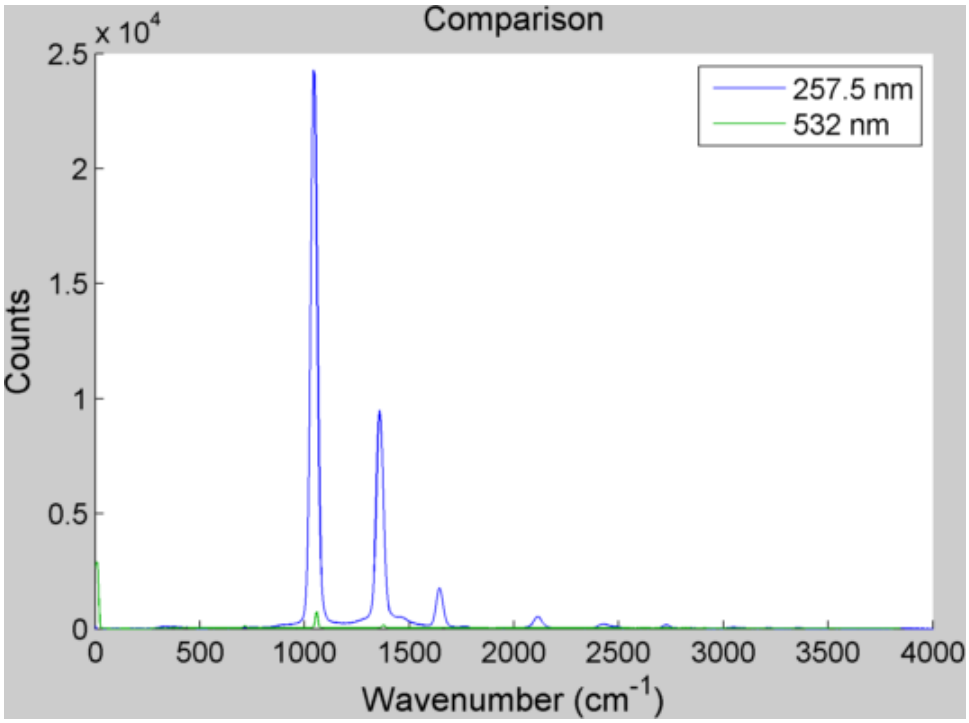

FIGURE 4.16: Comparison of Raman spectra for 257.5 nm and 532 nm

Figure 4.16 shows the comparison of Raman spectra of $NaNO_3$ for 257.5 and 532 nm. For the comparison, the differences in the efficiency of the diffraction gratings, filters and CCD for the the two wavelengths and the differences in the power were taken into account. For calculating the intensity ratio (Table 1), the counts from the figures were multiplied by hf, where h is the Planck constant and f is the frequency corresponding to the wavelength to get the intensity ratio.

The Table 1 gives the intensity ratio of $\frac{I_{257.5}}{I_{532}}$ for the Raman peaks.

Wavenumber cm^{-1}	$\frac{I_{257.5}}{I_{532}}$
1060	34.73
1376	75.53

An enhancement factor of greater than v_o^4 ratio is observed. Hence, we can see a resonant Raman effect for the $NaNO_3$ at 257.5 nm wavelength. This can be attributed to the increase in the absorption at 257.5 nm compared to that at 532 nm (Figure 4.17).

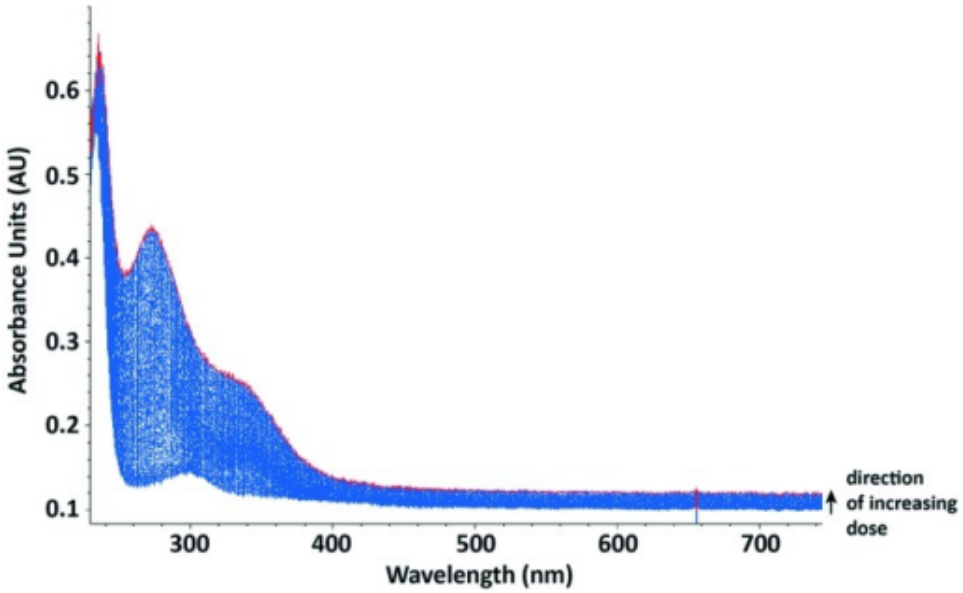

FIGURE 4.17: Absorption spectrum of 0.5 M sodium nitrate solution [17]

We are using $NaNO_3$ salt for the Raman spectra, so the concentration of $NaNO_3$ is high. It can be seen that the absorption at 257.5 nm is higher than that at 532 nm.

Chapter 5

Conclusion

We were able to show that, we can obtain fluorescence free Raman spectra for bio-molecules (oak leaf and lactobacillus acidophilus and bifidobacteria from a probotioc medicinal capsule). However the system is unable to resolve the important Raman peaks between 500 and 1600 cm^{-1}. The easiest way to resolve this issue is to procure a new grating with a higher groove density.

The other option is to redesign the spectrometer by changing the focal lengths of the focusing and the collimating mirrors to get a better resolution. We can also use a slit with a smaller width to further improve the resolution, but that also reduces the throughput, so may not be an ideal way to improve the resolution.

The last option is to optimize the laser system. Presently the FWHM of the laser is around 0.4 nm which is leading to FWHM of 60 cm^{-1} in wavenumber for Raman spectra. The issue seems to be the FWHM for 1030 nm wavelength is around 8 nm and this reduces to around 0.4 nm for 257.5 nm after performing SHG twice. The width at 1030 nm wavelength is around 8 nm due to self phase modulation (SPM) and the way to reduce the SPM is to reduce the peak power of the laser. Presently, the repetition rate is around 60 MHz, so, we are planning to increase the repetition rate to 80 Mhz to reduce the SPM [7]. This will help in obtaining a smaller bandwidth. It will also indirectly improve the power at 257.5 nm, as all the power is now contained in a smaller bandwidth. Higher power will also lead to a better signal to noise ratio for the Raman signal.

To establish an accurate comparison between the Raman signals obtained for 532 nm and 257.5 nm, we need to procure an objective and a focusing lens with chromatic aberration corrections. Presently, due to the lack of chromatic aberration corrections, the effective focal length changes with wavelength. This leads to a change in the amount of light collected by the objective. Due to the change in the effective focal length of the focusing lens, the slit position needs to be adjusted appropriately for 532 nm and 257.5 nm for obtaining the maximum Raman signal. This leads to a change in the amount of light coupling between the lens and spectrograph. The two lasers are aligned separately to get Raman signals. Therefore, any slight change in the alignment will lead to a change in the amount of the Raman signal being recorded. The fused silica plate used in the place of dichroic filter is the major contributor to the issue of change in alignment. It provides a different refractive index 1.5 for 257.5 nm and 1.46 for 532 nm which leads to a slight change in the path of the back scattered light being collected by the objective. This leads to a change in the alignment in terms of the position of the slit.

In the immediate future, we plan to acquire a grating with higher groove density and study more biological samples with deep UV Raman spectroscopy. In the future, we also plan to procure a custom made dichroic for UV, chromatically corrected optical components and optimize the design of the 257.5 nm laser.

Bibliography

[1] Raman , C.V., Krishnan, K.S.(1928). *The Optical Analogue of the Compton Effect* Nature, 121(3053), 711–711. http://doi.org/10.1038/121711a0

[2] Smekal, A. (1923). *Zur Quantentheorie der Dispersion.* Naturwissenschaften, 11(43), 873–875. http://doi.org/10.1007/BF01576902

[3] Asher, S. A. (1993). *UV Resonance Raman Spectroscopy for Analytical, Physical, and Biophysical Chemistry.* Anal. Chem., 65(4), 201A–210A. http://doi.org/10.1021/ac00052a715

[4] Asher, S. A., & Johnson, C. R. (1984). *Raman spectroscopy of a coal liquid shows that fluorescence interference is minimized with ultraviolet excitation.* Science, 225(4659), 311–3.

[5] Yazdi, Y., Ramanujam, N., Lotan, R., Mitchell, M. F., Hittelman, W., & Richards-Kortum, R. (1999). *Resonance Raman Spectroscopy at 257 nm Excitation of Normal and Malignant Cultured Breast and Cervical Cells.* Applied Spectroscopy, 53(1), 82–85. http://doi.org/10.1366/0003702991945254

[6] Wen, Z. Q., & Thomas, G. J. (1998). *UV resonance Raman spectroscopy of DNA and protein constituents of viruses: Assignments and cross sections for excitations at 257, 244, 238, and 229 nm.* Biopolymers, 45(3), 247–256.http://doi.org/10.1002/(SICI)1097-0282(199803)45:3<247::AID-BIP7>3.0.CO;2-R

[7] Oku, M., Kieu, K., & Peyghambarian, N. (2012). *High power all-fiber picosecond laser system for UV light generation* (p. 82371X). http://doi.org/10.1117/12.909190

[8] Szymanski, H. A. (Ed.). (1970). *Raman Spectroscopy.* Boston, MA: Springer US. Retrieved from http://link.springer.com/10.1007/978-1-4684-3027-1

[9] Johnson, B. B., & Peticolas, W. L. (1976). *The Resonant Raman Effect.* Annu. Rev. Phys. Chem., 27(1), 465–521. http://doi.org/10.1146/annurev.pc.27.100176.002341

[10] Beeman, D., Tsu, R.,& Thorpe, M. F. (1985). *Structural information from the Raman spectrum of amorphous silicon* Phys. Rev. B, 32(2), 874–878. http://doi.org/10.1103/PhysRevB.32.874

[11] Anastassakis, E., Pinczuk, A., Burstein, E., Pollak, F. H., Cardona, M. (1970). *Effect of static uniaxial stress on the Raman spectrum of silicon.* Solid State Commun., 8(2), 133–138. http://doi.org/10.1016/0038-1098(70)90588-0

[12] Sun, Q. (2009). *The Raman OH stretching bands of liquid water. Vib. Spectrosc.*, 51(2), 213–217. http://doi.org/10.1016/j.vibspec.2009.05.002

[13] Walrafen, G. E. (1962). *Raman Spectral Studies of the Effects of Electrolytes on Water.* The Journal of Chemical Physics, 36(4), 1035–1042. http://doi.org/10.1063/1.1732628

[14] Rao, A. M., Jorio, A., Pimenta, M. A., Dantas, M. S. S., Saito, R., Dresselhaus, G., & Dresselhaus, M. S. (2000). *Polarized Raman Study of Aligned Multiwalled Carbon Nanotubes.* Phys. Rev. Lett., 84(8), 1820–1823. http://doi.org/10.1103/PhysRevLett.84.1820

[15] Schulte, F., Lingott, J., Panne, U., & Kneipp, J. (2008). *Chemical Characterization and Classification of Pollen.* Anal. Chem., 80(24), 9551–9556. http://doi.org/10.1021/ac801791a

[16] Gaus, K., Rösch, P., Petry, R., Peschke, K.-D., Ronneberger, O., Burkhardt, H., … Popp, J. (2006). *Classification of lactic acid bacteria with UV-resonance Raman spectroscopy.* Biopolymers, 82(4), 286–290. http://doi.org/10.1002/bip.20448

[17] A stacked absorption spectrum of 0.5 M sodium nitrate solution. https://openi.nlm.nih.gov/detailedresult.php?img=PMC3526919_s-20-00023-fig3&query=null&uniq=1&req=4&simCollection=PMC3112332_fmicb-01-00128-g003&npos=113&prt=3